

Practical and optimal preparation of general quantum state with exponentially improved robustness

Xiao-Ming Zhang^{1,2,*}

¹*School of Physics, South China Normal University, Guangzhou 510006, China*

²*Center on Frontiers of Computing Studies, School of Computer Science, Peking University, Beijing 100871, China*

Quantum state preparation, as a general process of loading classical data to quantum device, is essential for end-to-end implementation of quantum algorithms. Yet, existing methods suffer from either complicated hardware or high circuit depth, limiting their robustness and also practicality. In this work, these limitations are overcome with a bucket-brigade approach. The tree architectures here represent the simplest connectivity required for achieving sub-exponential circuit depth. Leveraging the bucket-brigade mechanism that can suppress the error propagation between different branches, the approach exhibits exponential improvement in robustness compared to existing depth-optimal methods. More specifically, the infidelity scales as $O(\text{polylog}(N))$ with data size N , as opposed to $O(N)$ for conventional methods. Moreover, the approach here is the first to simultaneously achieve linear Clifford+ T circuit depth, gate count number, and space-time allocation. These advancements offer the opportunity for processing big data in both near-term and fault-tolerant quantum devices.

An end-to-end application of quantum algorithm requires the loading of classical data to a quantum device. Quantum state preparation, as a general classical data loading process, lies at the foundation of quantum algorithms. Given an $N = 2^n$ dimensional normalized vector $[\psi_0, \psi_1, \dots, \psi_{N-1}]$, quantum state preparation, from a trivial initial state $|0\rangle^{\otimes n}$, can be expressed as the following transformation

$$U_{\text{sp}}|0\rangle^{\otimes n} \otimes |\text{anc}\rangle = |\psi\rangle \otimes |\text{anc}\rangle, \quad (1)$$

where $|\psi\rangle \equiv \sum_{j=0}^{N-1} \psi_j |j\rangle$ is the target state, and $|\text{anc}\rangle$ represents the state of an ancillary system. The study of the quantum state preparation also has its fundamental motivations, as it indicates the space-time resource required to transform an arbitrary pure quantum state to another.

Various protocols have been proposed in the literature to realize Eq. (1), e.g. [1–14]. For example, Long, Sun [1] and Grover, Rudolph [2] have independently proposed iterative preparation methods based on multi-controlled-rotations. Subsequent works have improved the single- and two-qubit gate count to $O(N)$, which is optimal (e.g. [3, 4]). Although large gate count is inevitable in general, it is possible to trade time (circuit depth) for space (ancillary qubit). Recently, low-depth quantum state preparation with $\Theta(n)$ circuit depth that matches the lower bound has been achieved by several protocols [9–14], provided sufficient number of ancillary qubits. These results indicate an ultimate speed limit of loading general classical data to a quantum device.

Despite the remarkable progress of [9–14], current protocols are far from practical. On one hand, the robustness of [9–14] can not be guaranteed. The worst-case single- and two-qubit gate count of state preparation is $O(N)$, regardless of the space-time trade-off. A direct evaluation indicates that to achieve a constant preparation fidelity, one should suppress the gate error to the level of $O(N^{-1})$. For applications on large data sets, this requirement is too stringent to be practical, especially for near-term quantum devices. Even in the fault-tolerant setting, the gate error requirement of $O(N^{-1})$ is also challenging. Take the surface code [15] scheme as an example, the code distance of each logic qubit should increase polynomially with n , which

means that substantial portions of classical data processing and correction gates are required.

On the other hand, most of the existing protocols (e.g. [8–10, 12, 13]) assume full connectivity, which is not friendly for current quantum devices. In superconducting circuit systems, qubits are typically connected by couplers [16, 17], and only nearest neighbor interaction is available. There are other systems where better connectivity is available, such as trapped ions [18] and neutral-atom arrays [19]. However, simultaneous rearrangement of connectivities requires complicated shuttling, which is time-costly and may substantially affect the control accuracy. Although protocols in [11, 14] have sparse connectivity, the architecture is far from optimal.

Besides, the bucket-brigade quantum random access memory (QRAM) [20–26] enjoys both robustness and simple connectivity. The preliminary aim of QRAM protocols [20–26] is to perform the specific transformation

$$|j\rangle|0\rangle \rightarrow |j\rangle|D_j\rangle \quad (2)$$

coherently for $0 \leq j \leq N-1$, where D_j is binary data to be encoded, while the generalization to nonbinary D_j can be realized by adding a pointer [11]. Bucket-brigade QRAM stands out due to its provable noise resiliency [25, 27]. Moreover, qubits in this architecture are connected as a binary tree, and various schemes have been proposed to realize the Bucket-brigade QRAM in different systems, such as neutral atoms [21, 22], superconducting circuit [23], spin-photon network [28], etc. Unfortunately, Eq. (2) is only a special data loading process. QRAM per se is not sufficient for many applications. As a typical example, the block encoding of linear combinations of unitaries requires Eq. (2) sandwiched by Eq. (1) and its inverse [29]. While a general state preparation in Eq. (1) can be realized by iteratively querying multiple QRAMs, this naive approach has a large circuit depth overhead [increased to $O(n^2)$ as opposed to $O(n)$], and becomes much less robust.

In this work, inspired by the bucket-brigade mechanism, a novel fan-in process is developed to enable the optimal quantum state preparation Eq. (1). Compared to existing depth-

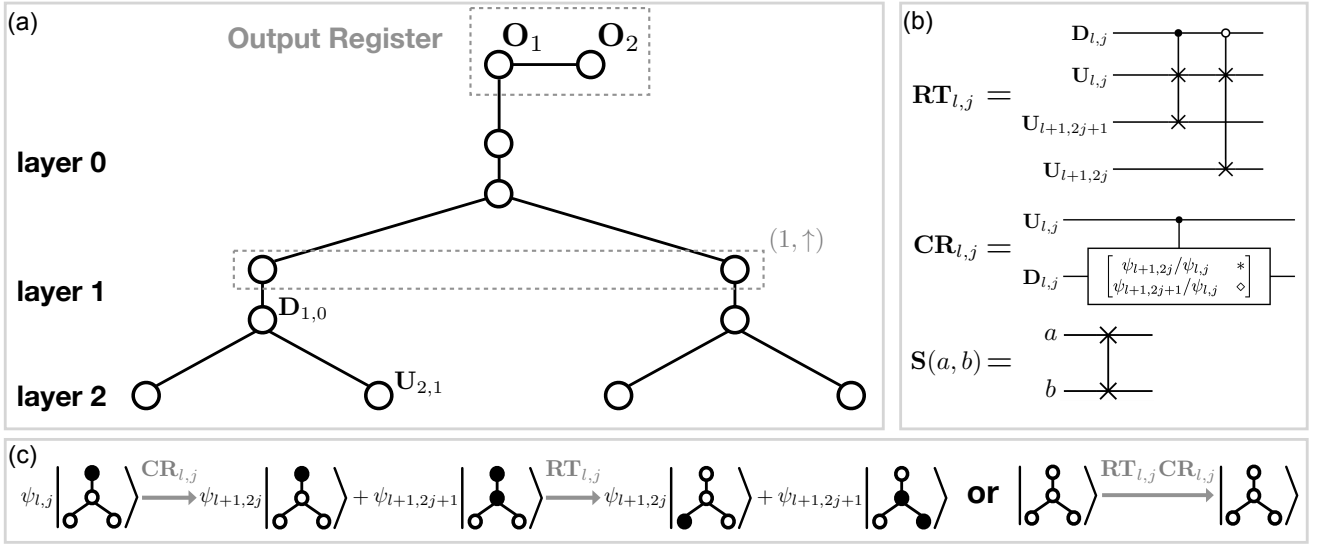


FIG. 1: (a) Hardware architecture of quantum state preparation protocols and corresponding notations in the main text. We take $n = 2$ as an example. Each circle represent a qubit, and each line represents to the connection between a pair of qubits. (b) Definitions of routing ($\mathbf{RT}_{l,j}$), controlled-rotations ($\mathbf{CR}_{l,j}$), and swap $\mathbf{S}(a, b)$ operations. In the operation $\mathbf{CR}_{l,j}$, labels $*$ and \diamond represent some values that make the matrix to be a unitary. (c) Sketch of how quantum state transforms during each operation in the fanin phase.

optimal methods [9–14], our approach overcome both the robustness and connectivity challenges, and at the same time improve the circuit complexity (see Table. I). In particular, the infidelity scaling is exponentially improved from $O(N)$ to $O(\text{polylog}(N))$ under fixed noise level. The hardware of our approach is as simple as the binary tree architecture, that each qubit connects to at most three of other qubits, which is optimal.

Two variations of the method is presented. The 2-qubit-per-node protocol is simpler while achieving optimal single- and two-qubit circuit complexity. The infidelity scales as $1 - F \leq A\epsilon n^3$ for some constant A and elementary gate error ϵ . Yet, its Clifford+ T circuit complexity is suboptimal. The more complex 3-qubit-per-node protocol has improved circuit complexity, and simultaneously achieve the best-known Clifford+ T gate count, circuit depth and space-time allocation (STA), i.e. sum of the individual duration that each qubit is active. It also improve the infidelity scaling to $1 - F \leq A\epsilon n^2$.

Below, we begin with the simple 2-qubit-per-node protocol.

Hardware architecture. As shown in Fig. 1, our 2-qubit-per-node protocol contains a bucket-brigade QRAM and an n -qubits output register. The bucket-brigade QRAM resembles an $(n + 1)$ layer binary tree and each node of the tree corresponds to two qubits. To be specific, the l th ($0 \leq l \leq n$) layer contains an upper and a lower sublayers, denoted as (l, \uparrow) and (l, \downarrow) respectively. An exception is that the leaf layer has only upper sublayers. Each sublayer contain totally 2^l qubits. We denote the j th qubit of (l, \uparrow) and (l, \downarrow) as $\mathbf{U}_{(l,j)}$ and $\mathbf{D}_{(l,j)}$. In QRAM, each qubit connects only to their parent or children. $\mathbf{U}_{l,j}$ has one child $\mathbf{D}_{l,j}$, and $\mathbf{D}_{l,j}$ for $l \neq n$ has two children $\mathbf{U}_{l+1,2j}$ and $\mathbf{U}_{l+1,2j+1}$. The output register contains n qubits,

each denoted as \mathbf{O}_j (from $j = 1$ to $j = n$). They are arranged as a line with nearest-neighbor coupling, and \mathbf{O}_1 also connect to the root of QRAM, i.e. $\mathbf{U}_{0,0}$. In this architecture, each qubit connects to at most 3 of the other qubits, which is optimal. This is because a graph of degree 2 can only form trivial lines or rings, qubit connections in such ways are insufficient for achieving subexponential circuit depth. It is worthy to note that similar to existing methods [9–14], the geometrically long-range interaction is fundamentally inevitable. In practice, the it can be realized by, for example, shuttling [18, 19] or teleported gates [11, 30, 31].

Fanin phase. In fanin phase, we only perform operations in QRAM. We begin with some notations of quantum states. Suppose \mathcal{S} is a set of qubits, we use the “activation” representation $|\mathcal{S}\rangle$ to represent that all qubits in \mathcal{S} is activated (i.e. at state $|1\rangle$), while all other qubits are at state $|0\rangle$. Formally, we have $|\mathcal{S}\rangle \equiv \otimes_{v \in \mathcal{V}^{\text{QRAM}}} |v \in \mathcal{S}\rangle_v$, where $|\cdot\rangle_v$ represents the state of qubit v , and the “True” or “False” result of $v \in \mathcal{S}$ correspond to the binary 1 or 0. $\mathcal{V}^{\text{QRAM}}$ represents all qubits in QRAM.

Let $|\psi_0\rangle = |\{\mathbf{U}_{0,0}\}\rangle$ be the initial state (i.e. only the root of QRAM is activated), we perform the following transformation

$$|\psi_l\rangle \longrightarrow |\psi_{l+1}\rangle, \quad |\psi_l\rangle \equiv \sum_{j=0}^{2^l-1} \psi_{l,j} |\mathcal{B}_{l,j}\rangle, \quad (3)$$

iteratively from $l = 0$ to $l = n - 1$, where $\psi_{l,j}$ will be defined later, and $\mathcal{B}_{l,j}$ is a set of qubits that will be clarified as follows. For qubit $\mathbf{D}_{(l,j)}$ at lower sublayers, we let $\mathcal{P}_{\downarrow}[\mathbf{D}_{(l,j)}] = \mathbf{D}_{(l-1, \lceil j/2 \rceil)}$ be its grandparent, which is also at the lower sublayers. Accordingly, we represent all ancestors of $\mathbf{D}_{(l,j)}$ in the

Algorithm 1 2-qubit-per-node quantum state preparation.

for $l = 0, \dots, n-1$:
 implement $\mathbf{PRT}_l \mathbf{PCR}_l$
for $m = 0$ to n :
 start $\mathbf{Fanout}(n-m)$
 idle for 3 steps

Algorithm 2 Subroutine $\mathbf{Fanout}(l)$

if $l \neq n$, implement \mathbf{PS}_l # takes 1 step
 implement $\mathbf{PRT}_{l-1,0}$ # takes l steps
if $l \neq n$, implement $\mathbf{S}(\mathbf{U}_{0,0}, \mathbf{O}_{l+1})$ # takes l steps
if $l = n$, $\mathbf{NOT}(\mathbf{U}_{0,0})$ # takes l steps

FIG. 2: Pseudo-codes of the 2-qubit-per-node quantum state preparation algorithms. Initial state of Algorithm 1 is $|\{\mathbf{U}_{0,0}\}\rangle$.

lower sublayers as $\mathcal{A}_{l,\downarrow,j} = \left\{ \mathcal{P}_{\downarrow}^{\otimes m} [\mathbf{D}_{(l,j)}] \mid 1 \leq m \leq l \right\}$, which contains totally l qubits. $|\mathcal{B}_{l,j}\rangle$ represents the following quantum state: at the subset of upper sublayers, only single qubit, $\mathbf{U}_{l,j}$, is activated and it serves as a *pointer*. At the subset of lower sublayers, $\mathcal{A}_{l,\downarrow,j}$ (all ancestors of $\mathbf{U}_{l,j}$ at lower sublayers) is at computational basis $|j_1 j_2 \dots j_l\rangle$, i.e. the first l bits of j . All other qubits are at state $|0\rangle$. The formal definition of $\mathcal{B}_{l,j}$ is

$$\mathcal{B}'_{l,j} = \{ \mathbf{D}_{l',j'} \in \mathcal{A}_{l,\downarrow,j} \mid j'_{l'} = 1 \} \quad (4a)$$

$$\mathcal{B}_{l,j} = \mathcal{B}'_{l,j} \cup \{ \mathbf{U}_{l,j} \}. \quad (4b)$$

which clarifies Eq. (3).

We then define $\psi_{l,j}$. Firstly, each amplitude may be represented as $\psi_j \equiv a_j \angle \phi_j$, where a_j and ϕ_j are absolute value and argument of ψ_j respectively. we set $\phi_0 = 0$ without loss of generality. Let $\psi_{n,j} \equiv \psi_j$, we recursively define $\psi_{l,j} = e^{i\phi_{l+1,2j}} \sqrt{a_{l+1,2j}^2 + a_{l+1,2j+1}^2}$.

We then turn to the gates required for this phase. Let $\mathbf{CR}_{l,j}$ be a controlled-rotation with $\mathbf{U}_{l,j}$ and $\mathbf{D}_{l,j}$ as controlled and target qubits, which satisfies (see also Fig. 1(b))

$$\mathbf{CR}_{l,j}|1\rangle \otimes (\psi_{l,j}|0\rangle) = |1\rangle \otimes (\psi_{l,2j}|0\rangle + \psi_{l,2j+1}|1\rangle) \quad (5a)$$

$$\mathbf{CR}_{l,j}|0\rangle \otimes |0\rangle = |0\rangle \otimes |0\rangle. \quad (5b)$$

Let $\mathbf{PCR}_l = \prod_{j=0}^{2^l-1} \mathbf{CR}_{l,j}$ be the parallel controlled-rotation, which can be realized with single layer of quantum circuit. This parallel rotation is crucial for data encoding.

Another critical operation is *routing*. Let $\mathbf{S}(a,b)$ be the swap gate between qubit a and b , routing is the following transformation

$$|0\rangle_{\text{rt}} \langle 0| \otimes \mathbf{S}(\text{in}, \text{lo}) + |1\rangle_{\text{rt}} \langle 1| \otimes \mathbf{S}(\text{in}, \text{ro}) \quad (6)$$

If the routing qubit (rt) is at state $|0\rangle$, we swap the states of incident qubit (in) and left output qubit (lo); if the routing

qubit is at state $|1\rangle$, we swap the states of input qubit and right output qubit (ro). We denote $\mathbf{RT}_{l,j}$ as the routing operation defined in Eq. (6) with $\mathbf{U}_{l,j}$, $\mathbf{D}_{l,j}$, $\mathbf{U}_{l,2j}$ and $\mathbf{U}_{l+1,2j+1}$ as the input, routing, left output and right output qubits respectively (see also Fig. 1(b)). Note that $\mathbf{RT}_{l,j}$ for different j can be implemented in parallel. Accordingly, we define $\mathbf{PRT}_l = \prod_{j=0}^{2^l-1} \mathbf{RT}_{l,j}$. This parallel routing can be implemented with constant circuit depth.

With elementary gates being explained, we are ready for discussing the transformation in Eq. (3). We first apply parallel controlled rotation \mathbf{PCR}_l . Except for qubit connected to the pointer (currently at $\mathbf{U}_{l,j}$), other qubits at sublayers (l, \downarrow) are not activated. So it can be verified that $\mathbf{PCR}_l(\psi_{l,j}|\mathcal{B}_{l,j}\rangle) = \psi_{l+1,2j}|\mathcal{B}_{l,j}\rangle + \psi_{l+1,2j+1}|\mathcal{B}_{l,j} \cup \{\mathbf{D}_{l,j}\}\rangle$. Then, we move the pointer from the l th to the $(l+1)$ th layer using parallel routing operation \mathbf{PRT}_l . Recall that $\mathbf{D}_{l,j}$ are controlled qubits of our routing operations. According to the property defined by Eq. (6), if $\mathbf{D}_{l,j}$ is not activated, the pointer moves to $\mathbf{D}_{l+1,2j}$, otherwise the pointer moves to $\mathbf{D}_{l+1,2j+1}$. Following the definition of $\mathcal{B}_{l,j}$, we have

$$\mathbf{PRT}_l|\mathcal{B}_{l,j}\rangle = |\mathcal{B}_{l+1,2j}\rangle \quad (7a)$$

$$\mathbf{PRT}_l|\mathcal{B}_{l,j} \cup \{\mathbf{D}_{l,j}\}\rangle = |\mathcal{B}_{l+1,2j+1}\rangle \quad (7b)$$

Combining with the recursive definition of $\psi_{l,j}$, we have $\mathbf{PCR}_l \mathbf{PRT}_l |\psi_l\rangle = |\psi_{l+1}\rangle$. Therefore, at the l th step, it suffices to implement $\mathbf{PCR}_l \mathbf{PRT}_l$ to realize the transformation in Eq. (3). A sketch about how quantum state transform during the operations is illustrated in Fig. 1(c).

Fanout stage. In this stage, our goal is to prepare the output register to the quantum state in Eq. (1), while uncompute the QRAM. In other words, we perform the basis transformation $|\mathcal{B}_{n,j}\rangle|0 \dots 0\rangle_{\text{out}} \rightarrow |\emptyset\rangle|j\rangle_{\text{out}}$, where $|\cdot\rangle_{\text{out}}$ is the quantum state of output register in binary representation, while the state of QRAM is still in activation representation. This transformation has been introduced in [25] for binary data, and subsequently been generalized to continuous data by adding an extra pointer [11]. The fanout stage is as follows.

We define the shorthand $\mathbf{PRT}_{a:b} \equiv \mathbf{PRT}_a \dots \mathbf{PRT}_{b+1} \mathbf{PRT}_b$ for some $b > a$. We first perform operation $\mathbf{PRT}_{0:n-1}$. The pointer then moved to the root of the QRAM, i.e. $\mathbf{PRT}_{0:n-1}|\mathcal{B}_{n,j}\rangle = |\mathcal{A}_{n,\downarrow,j} \cup \{\mathbf{U}_{0,0}\}\rangle$ for arbitrary j . So we can then apply $\mathbf{NOT}(\mathbf{U}_{0,1})$ (i.e. NOT gate at qubit $\mathbf{U}_{0,0}$) to uncompute the pointer. After this step, the basis $|\mathcal{B}_{n,j}\rangle|0 \dots 0\rangle_{\text{out}}$ has been transferred to $|\mathcal{B}'_{n,j}\rangle|0 \dots 0\rangle_{\text{out}}$.

We then define

$$|\Psi_{l,j}\rangle = |\mathcal{B}'_{l,j;l}\rangle \otimes |0 \dots 0 j_{l+1} \dots j_n\rangle_{\text{out}}. \quad (8)$$

The current basis and target basis corresponds to $l = n$ and $l = 0$ respectively. We will then perform the basis transformation $|\Psi_{l+1,j}\rangle \rightarrow |\Psi_{l,j}\rangle$ iteratively. We define $\mathbf{PS}_l = \prod_{j=1}^{2^l} \mathbf{S}(\mathbf{U}_{l,j}, \mathbf{D}_{l,j})$ as the parallel swap gate applied between sublayers (l, \uparrow) and (l, \downarrow) . By applying \mathbf{PS}_l to

TABLE I: Comparison to some typical state preparation protocols with $\tilde{O}(n)$ circuit depth. The estimation of infidelity scalings for [9, 11, 13, 14] are based on direct counting of the total gate counts.

Protocols	Infidelity scaling	Connectivity	Count	Depth	STA
Ref [9]	N	all-to-all	$O(N \log(N/\varepsilon))$	$O(n \log(N/\varepsilon))$	$O(Nn \log(N/\varepsilon))$
Ref [11, 14]	N	degree 4	$O(N \log(\mathbf{1}/\varepsilon))$	$O(n \log(n/\varepsilon))$	$O(Nn \log(n/\varepsilon))$
Ref [13]	N	all-to-all	$O(N \log(n/\varepsilon))$	$O(\mathbf{n} + \log(\mathbf{1}/\varepsilon))$	$O(N \log(n/\varepsilon))$
2-qubit-per-node	n^3	degree 3	$O(N \log(\mathbf{1}/\varepsilon))$	$O(n \log(n/\varepsilon))$	$O(N \log(n/\varepsilon))$
3-qubit-per-node	\mathbf{n}^2	degree 3	$O(N \log(\mathbf{1}/\varepsilon))$	$O(\mathbf{n} + \log(\mathbf{1}/\varepsilon))$	$O(N \log(\mathbf{1}/\varepsilon))$

$|\Psi_{l+1}\rangle$, activation at sublayer (l, \downarrow) are transferred to sublayers (l, \uparrow) . We then implement routing $\mathbf{PRT}_{l-1:0}$, after which the sublayer (l, \uparrow) is uncomputed, while the root of QRAM is prepared at state $|j_{n-l}\rangle$. Therefore, by further performing swap gate $\mathbf{S}(\mathbf{U}_{0,0}, \mathbf{O}_{l+1})$, we complete the transformation. Note that $\mathbf{S}(\mathbf{U}_{0,0}, \mathbf{O}_{l+1})$ is a non-local operation, which should be decomposed into totally $(l+1)$ steps of local swap gates applied at pairs of connected qubits. To conclude, let $\mathbf{Fanout}(l) \equiv \mathbf{S}(\mathbf{U}_{0,1}, \mathbf{O}_{l+1})\mathbf{PRT}_{l-1:0}\mathbf{PS}_l$ (see algorithm. 2 in Fig. 2), we have

$$\mathbf{Fanout}(l)|\Psi_{l+1}\rangle = |\Psi_l\rangle \quad (9)$$

for $0 \leq l \leq n-1$. Transformation $\mathbf{Fanout}(l)$ has circuit depth $O(l)$. If we naively implement Eq. (9) for different l sequentially, the total circuit depth is $O(n^2)$. Fortunately, $\mathbf{Fanout}(l-1)$ does not need to start after $\mathbf{Fanout}(l)$ finish. In fact, after the third step of $\mathbf{Fanout}(l)$ (one swap gate and two parallel routing), state $|j_l\rangle$ has already been routed to layer $(l-2, \uparrow)$ (or into the output register for small l). If we now start $\mathbf{Fanout}(l-1)$, the subsequent operations in $\mathbf{Fanout}(l)$ and $\mathbf{Fanout}(l-1)$ with not affect each other. Therefore, our fanout stage works as follows (see also Algorithm. 1 in Fig. 2). We start the uncomputation of pointer (denoted as $\mathbf{Fanout}(n)$). Then, from $l = n-1$ to $l = 0$, we idle for 3 steps and then start the $\mathbf{Fanout}(l)$. In this way, the fanout process contains totally $(4n+3)$ steps, so the circuit depth of the fanout process, and also the entire state preparation process, is $O(n)$. This result improves the naive approach of querying Eq. (2) for n times (which has $O(n^2)$ circuit depth), and achieve the optimal single- and two-qubit circuit complexity.

Robustness. One of the crucial advantages of bucket-brigade architecture is the noise resiliency. It has been shown that the error of bucket-brigade QRAM scales only polylogarithmically with n for Eq. (2) with binary $|D_j\rangle$. Because we are using a similar hardware architecture, it is expected that our state preparation protocol also enjoys the similar noise resiliency.

In Sec. I of [32], it is shown that this is the case. In particular, we consider the local depolarization model that is standard in the noisy quantum circuit study [33–35], although the results in this work are expected to be also valid for more general scenarios. The specific model is as follows, after each layer of the elementary single- and two-qubit gates, depolarization

channel $(1-\varepsilon)\mathcal{I} + \varepsilon/3(\mathcal{X} + \mathcal{Y} + \mathcal{Z})$ is applied on *all* qubits with fixed ε , where \mathcal{X} , \mathcal{Y} , \mathcal{Z} and \mathcal{I} are single qubit Pauli X , Y , Z and I channels respectively. Under local Pauli noise, the state preparation infidelity for Algorithm.1 in Fig. 2 satisfies $1-F \leq A\varepsilon n^3$ for some constant A . As a comparison, for a general quantum circuit with $O(2^n)$ elementary gates, the total infidelity scales exponentially with n .

The main idea of our proof about noise robustness is as follows. The noisy circuit can be decomposed into the linear combination of unitary evolutions, and each unitary evolution represents a specific space-time error configuration c . By a careful analysis on how error propagates between different branches of the QRAM, the final output state can be expressed as $|\tilde{\psi}(c)\rangle_{\text{out}} = \sum_{j \in g'(c)} \psi_j |f(c)\rangle_{\text{qram}} \otimes |j\rangle_{\text{out}} + |\text{garb}\rangle$. Where $g'(c)$ represents some *error-free* branches that error will never propagate into it and $|\text{garb}\rangle$ is an unnormalized garbage state orthogonal to the first term. An important fact is that after tracing out QRAM part of $|\tilde{\psi}(c)\rangle_{\text{out}}$, the infidelity satisfies $1-F(c) \leq \sum_{j \in g'(c)} |\psi_j|^2 \equiv \Lambda'(c)$. In sampling different error configuration c , we have $\mathbb{E}[\Lambda'(c)] \geq (1-A\varepsilon n^3)$. The cubic infidelity scaling then follows from the concavity of fidelity.

3-qubit-per-node protocol. The Clifford+ T complexity, which is important for fault-tolerant implementation, is not yet optimal for the protocol above. In [32], it is shown that the fault-tolerant performance can be further improved with our 3-qubit-per-node protocol. In this architecture, a middle sublayer is inserted between (l, \uparrow) and (l, \downarrow) , while each qubit is still connect to at most 3 other qubits. One of the advantage is that we can use the pre-rotation [13] technique, i.e. rotations encoding amplitudes ψ_j are implemented prior to the routing operations. This allows us to simultaneously achieve the linear Clifford+ T circuit depth, gate count number and space-time allocation (see Tabel. I). More importantly, the 3-qubit-per-node protocol can further improve the noise robustness. All routing operations should be controlled by extra pointer qubits in the middle sublayers. This revision can block all the error propagation from bad branches to good branches, and hence improve the infidelity to

$$1-F \leq A\varepsilon n^2. \quad (10)$$

It is worthy to note that a similar idea is also applicable to improve the robustness of qubit-based QRAM in Eq. (2). More specifically, it is known that *qutrit*-based QRAMs has

quadratic infidelity scaling. By replacing the qutrits by the combination of two qubits, one can improve the infidelity scaling from cubic to quadratic for Eq. (2). Yet, our protocol for Eq. (1) is more than this replacement, because the pre-rotation technique [13] enables the further improvement of Clifford+ T complexities.

Outlooks While we have only considered Pauli depolarization channel here, it is expected that the protocol is robust for general quantum noise models (e.g. dephasing, decaying), in case the error is not a catastrophe one applied globally. Moreover, the robustness mechanism here is applicable to other type of data loading process, such as the linear combination of unitaries [29, 36–38], sparse-access input model [38–44], function loading [45, 46] etc. It also serve as a promising candidate for future quantum data center [47, 48]. In experimental aspect, our protocol is directly implementable in state-of-the-art quantum platforms [18, 19, 31].

Acknowledgement. The author thank Alexander Denzel, Connor T. Hann and Xiao Yuan for helpful discussions. This work is supported by National Natural Science Foundation of China (No. 12405013).

* Electronic address: phyxzm@gmail.com

- [1] G.-L. Long and Y. Sun, Efficient scheme for initializing a quantum register with an arbitrary superposed state, *Phys. Rev. A* **64**, 014303 (2001).
- [2] L. Grover and T. Rudolph, Creating superpositions that correspond to efficiently integrable probability distributions, Preprint at <https://arxiv.org/abs/quant-ph/0208112> (2002).
- [3] M. Möttönen, J. J. Vartiainen, V. Bergholm, and M. M. Salomaa, Transformation of quantum states using uniformly controlled rotations, *Quantum. Inf. Comput.* **5**, 467 (2005).
- [4] M. Plesch and Č. Brukner, Quantum-state preparation with universal gate decompositions, *Phys. Rev. A* **83**, 032302 (2011).
- [5] G. H. Low, V. Kliuchnikov, and L. Schaeffer, Trading t gates for dirty qubits in state preparation and unitary synthesis, *Quantum* **8**, 1375 (2024).
- [6] Z. Zhang, Q. Wang, and M. Ying, Parallel quantum algorithm for hamiltonian simulation, *Quantum* **8**, 1228 (2024).
- [7] X.-M. Zhang, M.-H. Yung, and X. Yuan, Low-depth quantum state preparation, *Phys. Rev. Res.* **3**, 043200 (2021).
- [8] B. D. Clader, A. M. Dalzell, N. Stamatopoulos, G. Salton, M. Berta, and W. J. Zeng, Quantum resources required to block-encode a matrix of classical data, *IEEE Transactions on Quantum Engineering* **3**, 1 (2022).
- [9] X. Sun, G. Tian, S. Yang, P. Yuan, and S. Zhang, Asymptotically optimal circuit depth for quantum state preparation and general unitary synthesis, *IEEE Transactions on Computer-Aided Design of Integrated Circuits and Systems* (2023).
- [10] G. Rosenthal, Query and depth upper bounds for quantum unitaries via grover search, Preprint at <https://arxiv.org/abs/2111.07992> (2021).
- [11] X.-M. Zhang, T. Li, and X. Yuan, Quantum state preparation with optimal circuit depth: Implementations and applications, *Phys. Rev. Lett.* **129**, 230504 (2022).
- [12] P. Yuan and S. Zhang, Optimal (controlled) quantum state preparation and improved unitary synthesis by quantum circuits with any number of ancillary qubits, *Quantum* **7**, 956 (2023).
- [13] K. Gui, A. M. Dalzell, A. Achille, M. Suchara, and F. T. Chong, Spacetime-efficient low-depth quantum state preparation with applications, *Quantum* **8**, 1257 (2024).
- [14] X.-M. Zhang and X. Yuan, Circuit complexity of quantum access models for encoding classical data, *npj Quantum Information* **10**, 42 (2024).
- [15] A. G. Fowler, M. Mariantoni, J. M. Martinis, and A. N. Cleland, Surface codes: Towards practical large-scale quantum computation, *Phys. Rev. A* **86**, 032324 (2012).
- [16] F. Arute, K. Arya, R. Babbush, D. Bacon, J. C. Bardin, R. Barends, R. Biswas, S. Boixo, F. G. Brandao, D. A. Buell, *et al.*, Quantum supremacy using a programmable superconducting processor, *Nature* **574**, 505 (2019).
- [17] Y. Wu, W.-S. Bao, S. Cao, F. Chen, M.-C. Chen, X. Chen, T.-H. Chung, H. Deng, Y. Du, D. Fan, *et al.*, Strong quantum computational advantage using a superconducting quantum processor, *Physical review letters* **127**, 180501 (2021).
- [18] S. A. Moses, C. H. Baldwin, M. S. Allman, R. Ancona, L. Ascarunz, C. Barnes, J. Bartolotta, B. Bjork, P. Blanchard, M. Bohn, *et al.*, A race-track trapped-ion quantum processor, *Physical Review X* **13**, 041052 (2023).
- [19] D. Bluvstein, S. J. Evered, A. A. Geim, S. H. Li, H. Zhou, T. Manovitz, S. Ebadi, M. Cain, M. Kalinowski, D. Hangleiter, *et al.*, Logical quantum processor based on reconfigurable atom arrays, *Nature* **626**, 58 (2024).
- [20] V. Giovannetti, S. Lloyd, and L. Maccone, Quantum random access memory, *Phys. Rev. Lett.* **100**, 160501 (2008).
- [21] V. Giovannetti, S. Lloyd, and L. Maccone, Architectures for a quantum random access memory, *Phys. Rev. A* **78**, 052310 (2008).
- [22] F.-Y. Hong, Y. Xiang, Z.-Y. Zhu, L.-z. Jiang, and L.-n. Wu, Robust quantum random access memory, *Phys. Rev. A* **86**, 010306 (2012).
- [23] C. T. Hann, C.-L. Zou, Y. Zhang, Y. Chu, R. J. Schoelkopf, S. M. Girvin, and L. Jiang, Hardware-efficient quantum random access memory with hybrid quantum acoustic systems, *Phys. Rev. Lett.* **123**, 250501 (2019).
- [24] T. M. Veras, I. C. De Araujo, K. D. Park, and A. J. Dasilva, Circuit-based quantum random access memory for classical data with continuous amplitudes, *IEEE Trans. Comput.* **70**, 2125 (2021).
- [25] C. T. Hann, G. Lee, S. Girvin, and L. Jiang, Resilience of quantum random access memory to generic noise, *PRX Quantum* **2**, 020311 (2021).
- [26] S. Jaques and A. G. Rattew, Qram: A survey and critique, Preprint at <https://arxiv.org/abs/2305.10310> (2023).
- [27] S. Arunachalam, V. Gheorghiu, T. Jochym-O'Connor, M. Mosca, and P. V. Srinivasan, On the robustness of bucket brigade quantum ram, *New Journal of Physics* **17**, 123010 (2015).
- [28] K. C. Chen, W. Dai, C. Errando-Herranz, S. Lloyd, and D. Englund, Scalable and high-fidelity quantum random access memory in spin-photon networks, *PRX Quantum* **2**, 030319 (2021).
- [29] G. H. Low and I. L. Chuang, Hamiltonian simulation by qubitization, *Quantum* **3**, 163 (2019).
- [30] D. Gottesman and I. L. Chuang, Demonstrating the viability of universal quantum computation using teleportation and single-qubit operations, *Nature* **402**, 390 (1999).
- [31] K. S. Chou, J. Z. Blumoff, C. S. Wang, P. C. Reinhold, C. J. Axline, Y. Y. Gao, L. Frunzio, M. Devoret, L. Jiang, and R. Schoelkopf, Deterministic teleportation of a quantum gate between two logical qubits, *Nature* **561**, 368 (2018).

- [32] See Supplemental Material.
- [33] S. Boixo, S. V. Isakov, V. N. Smelyanskiy, R. Babbush, N. Ding, Z. Jiang, M. J. Bremner, J. M. Martinis, and H. Neven, Characterizing quantum supremacy in near-term devices, *Nature Physics* **14**, 595 (2018).
- [34] S. Bravyi, D. Gosset, R. König, and M. Tomamichel, Quantum advantage with noisy shallow circuits, *Nature Physics* **16**, 1040 (2020).
- [35] D. Aharonov, X. Gao, Z. Landau, Y. Liu, and U. Vazirani, A polynomial-time classical algorithm for noisy random circuit sampling, in *Proceedings of the 55th Annual ACM Symposium on Theory of Computing* (2023) pp. 945–957.
- [36] L. Gui-Lu, General quantum interference principle and duality computer, *Communications in Theoretical Physics* **45**, 825 (2006).
- [37] A. M. Childs and N. Wiebe, Hamiltonian simulation using linear combinations of unitary operations, Preprint at <https://arxiv.org/abs/1202.5822> (2012).
- [38] S. Chakraborty, A. Gilyén, and S. Jeffery, The power of block-encoded matrix powers: Improved regression techniques via faster hamiltonian simulation, in *Proceedings of the 46th International Colloquium on Automata, Languages and Programming (ICALP)* (2019).
- [39] D. W. Berry, G. Ahokas, R. Cleve, and B. C. Sanders, Efficient quantum algorithms for simulating sparse hamiltonians, *Communications in Mathematical Physics* **270**, 359 (2007).
- [40] A. M. Childs and R. Kothari, Simulating sparse hamiltonians with star decompositions, in *Theory of Quantum Computation, Communication, and Cryptography: 5th Conference, TQC 2010, Leeds, UK, April 13-15, 2010, Revised Selected Papers 5* (Springer, 2011) pp. 94–103.
- [41] A. M. Childs, On the relationship between continuous-and discrete-time quantum walk, *Communications in Mathematical Physics* **294**, 581 (2010).
- [42] D. W. Berry, A. M. Childs, R. Cleve, R. Kothari, and R. D. Somma, Exponential improvement in precision for simulating sparse hamiltonians, in *Proceedings of the forty-sixth annual ACM symposium on Theory of computing* (2014) pp. 283–292.
- [43] A. W. Harrow, A. Hassidim, and S. Lloyd, Quantum algorithm for linear systems of equations, *Phys. Rev. Lett.* **103**, 150502 (2009).
- [44] A. M. Childs, R. Kothari, and R. D. Somma, Quantum algorithm for systems of linear equations with exponentially improved dependence on precision, *SIAM J. Comput.* **46**, 1920 (2017).
- [45] G. Marin-Sanchez, J. Gonzalez-Conde, and M. Sanz, Quantum algorithms for approximate function loading, arXiv:2111.07933 (2021).
- [46] A. G. Rattew and B. Koczor, Preparing arbitrary continuous functions in quantum registers with logarithmic complexity, arXiv:2205.00519 (2022).
- [47] J. Liu, C. T. Hann, and L. Jiang, Data centers with quantum random access memory and quantum networks, *Physical Review A* **108**, 032610 (2023).
- [48] J. Liu and L. Jiang, Quantum data center: Perspectives, Preprint at <https://arxiv.org/abs/2309.06641> (2023).
- [49] P. Selinger, Efficient clifford+t approximation of single-qubit operators, Preprint at <https://arxiv.org/abs/1212.6253> (2012).

Supplemental material

Contents

References	5
I. Robustness analysis for 2-qubit-per-node protocol	7
A. noise model	7
B. Linear combination of unitary evolutions	8
C. Definition of good branch	9
D. Fanin phase	9
E. Fanout phase	10
F. State preparation infidelity	12
II. 3-qubit-per-node protocol	13
A. Hardware architecture and basic operations	13
B. Fanin phase	13
C. Fanout phase	15
D. Robustness analysis	16
E. Clifford+ T decomposition	17
1. Decomposition protocol and error analysis	17
2. Circuit complexity	18

I. ROBUSTNESS ANALYSIS FOR 2-QUBIT-PER-NODE PROTOCOL

A. noise model

As explained in the main text, state preparation protocol contains totally $O(n)$ layers of quantum circuit. We can abstractly expressed the quantum circuit as $\prod_{m=1}^M U_m |\psi_{\text{ini}}\rangle = |\psi_{\text{targ}}\rangle$, where U_m is the m th layer of single- and two-qubit gates. The specific form of U_m depends on how we decompose the operations (e.g. elementary routing and control rotation operations), but we typically have $M = O(n)$. In practice, we should deal with mixed state due to the existence of noise, so we also define the corresponding unitary channels as $\mathcal{U}_m[\cdot] = U_m[\cdot]U_m^\dagger$. Let

$$\mathcal{U} = \mathcal{U}_M \circ \cdots \circ \mathcal{U}_2 \circ \mathcal{U}_1 \quad (\text{S-1})$$

be the ideal evolution, we have $\mathcal{U}[\rho_{\text{ini}}] = \rho_{\text{end}}$, where $\rho_{\text{ini}} = |\psi_{\text{ini}}\rangle\langle\psi_{\text{ini}}|$, and $\rho_{\text{end}} = |\psi_{\text{end}}\rangle\langle\psi_{\text{end}}|$ are initial and ideal output state. Let $\rho_{\text{id}} = |\psi\rangle\langle\psi|$ be the target state of the quantum state preparation, we have $\rho_{\text{id}} = \text{Tr}_{\text{qram}}[\rho_{\text{end}}]$, where Tr_{qram} is the partial trace over the QRAM.

We then introduce the local depolarization noise model. We define

$$\mathcal{E}_q = (1 - \varepsilon)I + \frac{1}{3}\varepsilon (\mathcal{X}_q + \mathcal{Y}_q + \mathcal{Z}_q) \quad (\text{S-2})$$

as the noisy quantum channel applied at qubit q , where $\varepsilon \in (0, 1)$ is the error probability, $I[\rho] = \rho$, $\mathcal{X}[\rho] = X_q \rho X_q$, $\mathcal{Y}[\rho] = Y_q \rho Y_q$, $\mathcal{Z}[\rho] = Z_q \rho Z_q$, are Pauli I , X , Y and Z channels applied at qubit q respectively. After the implementation of each layer of quantum circuit \mathcal{U}_m , \mathcal{E}_q is applied at all qubits in the system. In other words, let $\mathcal{E} \equiv \prod_{q \in \mathcal{V}} \mathcal{E}_q$, where \mathcal{V} is the set of all qubits in both QRAM and output register, the ideal channel \mathcal{U}_m is replaced by the noisy channel $\tilde{\mathcal{U}}_m = \mathcal{E} \circ \mathcal{U}_m$. So the noisy quantum state preparation can be described by the following quantum channel

$$\tilde{\mathcal{U}} \equiv \tilde{\mathcal{U}}_M \circ \cdots \circ \tilde{\mathcal{U}}_2 \circ \tilde{\mathcal{U}}_1. \quad (\text{S-3})$$

B. Linear combination of unitary evolutions

We then show how to decompose $\tilde{\mathcal{U}}$ into the linear combination of unitary evolutions. We first rewrite \mathcal{E} as the linear combination of all possible qubit distribution of error

$$\mathcal{E} \equiv \sum_{Q \in \text{Power}(\mathcal{V})} \mathcal{E}_Q \equiv \sum_{Q \in \text{Power}(\mathcal{V})} p_Q \mathcal{D}_Q, \quad (\text{S-4})$$

where $\text{Power}(\mathcal{V})$ is the power of \mathcal{V} , i.e. all possible subset of all qubits. Moreover, $\mathcal{D}_q = \mathcal{X}_q + \mathcal{Y}_q + \mathcal{Z}_q$ represents the depolarization part of Eq. (S-2), and $\mathcal{D}_Q = \prod_{q \in Q} \mathcal{D}_q$, $p_Q = (1 - \varepsilon)^{|\mathcal{V}| - |Q|} \varepsilon^{|Q|}$. Here, \mathcal{D}_Q represents that errors are applied at qubits in set Q while all qubits not in Q is free of errors. The probability distribution p_Q is normalized, and decreases with $|Q|$.

Then, let $\mathcal{Q} \equiv [Q_1, \dots, Q_M]$ be a vector of qubit set for some $Q_m \in \text{Power}(\mathcal{V})$. \mathcal{Q} describes a specific space-time configuration of the depolarization error. More specifically, we define

$$\tilde{\mathcal{U}}(\mathcal{Q}) = \mathcal{D}_{Q_M} \circ \mathcal{U}_M \circ \dots \circ \mathcal{D}_{Q_2} \circ \mathcal{U}_2 \circ \mathcal{D}_{Q_1} \circ \mathcal{U}_1, \quad (\text{S-5})$$

and $p_{\mathcal{Q}} = \prod_{m=1}^M p_{Q_m}$. Let $\mathcal{Q} = \{[Q_1, \dots, Q_M] | Q_m \in \text{Power}(\mathcal{V}) \text{ for all } 1 \leq m \leq M\}$ be all possible space-time configuration, we can rewrite $\tilde{\mathcal{U}}$ in Eq. (S-3) as

$$\tilde{\mathcal{U}} = \sum_{\mathcal{Q} \in \mathcal{Q}} p_{\mathcal{Q}} \tilde{\mathcal{U}}(\mathcal{Q}). \quad (\text{S-6})$$

We further decompose each $\tilde{\mathcal{U}}(\mathcal{Q})$ into the linear combination of unitary evolutions. Recall that in Eq. (S-5), each depolarization \mathcal{D}_{Q_m} is the linear combination of three unitary channels. Let $\mathcal{P}_{Q_m} = \{\prod_{q \in Q_m} \mathcal{P}_q | \mathcal{P}_q \in \{\mathcal{X}_q, \mathcal{Y}_q, \mathcal{Z}_q\}\}$, we have

$$\mathcal{D}_{Q_m} = \frac{1}{|\mathcal{P}_{Q_m}|} \sum_{\mathcal{P} \in \mathcal{P}_{Q_m}} \mathcal{P}, \quad (\text{S-7})$$

where $|\mathcal{P}_{Q_m}| = 3^{|Q_m|}$. Let $[\mathcal{P}_1, \mathcal{P}_2, \dots, \mathcal{P}_M]$ be the polarization configuration of errors, we define all possible $[\mathcal{P}_1, \mathcal{P}_2, \dots, \mathcal{P}_M]$ under a space-time configuration \mathcal{Q} as $\mathcal{P}_{\mathcal{Q}} \equiv \{[\mathcal{P}_1, \mathcal{P}_2, \dots, \mathcal{P}_M] | \mathcal{P}_m \in \mathcal{P}_{Q_m}\}$. $\tilde{\mathcal{U}}(\mathcal{Q})$ can therefore be decomposed as

$$\tilde{\mathcal{U}}(\mathcal{Q}) = \frac{1}{|\mathcal{P}_{\mathcal{Q}}|} \sum_{c \in \mathcal{P}_{\mathcal{Q}}} \tilde{\mathcal{U}}(c), \quad (\text{S-8})$$

where c represents a specific space-time-polarization configuration of error, and

$$\tilde{\mathcal{U}}([\mathcal{P}_1, \mathcal{P}_2, \dots, \mathcal{P}_M]) \equiv \mathcal{P}_M \mathcal{U}_M \dots \mathcal{P}_2 \mathcal{U}_2 \mathcal{P}_1 \mathcal{U}_1. \quad (\text{S-9})$$

Because each \mathcal{P}_m is a unitary channel, Eq. (S-9) is also a unitary channel. The total noisy evolution can then be decomposed as the linear combination of unitary evolutions as

$$\tilde{\mathcal{U}} = \sum_{\mathcal{Q} \in \mathcal{Q}} \sum_{c \in \mathcal{P}_{\mathcal{Q}}} p_c \tilde{\mathcal{U}}(c) \quad (\text{S-10})$$

for some $p_c = p_{\mathcal{Q}} / |\mathcal{P}_{\mathcal{Q}}|$. Let

$$\tilde{\rho}_{\text{out}}(c) = \text{Tr}_{\text{gram}} [\tilde{\mathcal{U}}(c) [\rho_{\text{ini}}]], \quad (\text{S-11})$$

the final noisy output state is therefore $\tilde{\rho}_{\text{out}} = \sum_c p_c \tilde{\rho}_{\text{out}}(c)$, where the some is over all possible space-time-polarization configurations. We denote $\text{Fid}(A, B)$ as the fidelity between two density matrices A and B , the total state preparation fidelity is just $F \equiv \text{Fid}(\rho_{\text{id}}, \tilde{\rho}_{\text{out}})$. Due to the concavity of fidelity, we have

$$\begin{aligned} F &\geq \sum_{\mathcal{Q} \in \mathcal{Q}} \sum_{c \in \mathcal{P}_{\mathcal{Q}}} p_c \text{Fid}[\rho_{\text{id}}, \tilde{\rho}_{\text{out}}(c)] \\ &= \mathbb{E} [\text{Fid}(\rho_{\text{id}}, \tilde{\rho}_{\text{out}}(c))]. \end{aligned} \quad (\text{S-12})$$

where $\mathbb{E}[\cdot]$ represents the expectation value with c sampled according to p_c . The remaining of this section is to study the unitary evolution under space-time-depolarization configuration c , and estimate Eq. (S-12).

C. Definition of good branch

Before discussing the infidelity of $\tilde{\rho}_{\text{out}}(c)$, we give the definition of *good* branch and related terminologies that are useful. To begin with, we define the parent of each node as

$$\text{Parent}[X] = \begin{cases} \mathbf{O}_{l+1} & X = \mathbf{O}_l \text{ for } 1 \leq l \leq n-1 \\ \mathbf{O}_0 & X = \mathbf{U}_{0,1} \\ \mathbf{D}_{(l-1, \lceil j/2 \rceil)} & X = \mathbf{U}_{(l,j)} \text{ for some } l \neq 0 \\ \mathbf{U}_{(l,j)} & X = \mathbf{D}_{(l,j)} \text{ for some } l \neq 0 \end{cases} \quad (\text{S-13})$$

Note that $\text{Parent}[\cdot]$ does not have definition for \mathbf{O}_n . We then define $\mathcal{A}_{l,j}$ as all ancestors of qubit $\mathbf{U}_{l,j}$ as

$$\mathcal{A}_{l,j} = \{\text{Parent}^{\text{ot}}[\mathbf{U}_{l,j}] \mid 1 \leq t \leq 3n\}. \quad (\text{S-14})$$

Let $\mathcal{A}_{l,j}^{(\text{neighbor})}$ be the set of all the nearest-neighbor qubits of qubits in $\mathcal{A}_{l,j}$, and

$$\hat{\mathcal{A}}_{l,j} = \mathcal{A}_{l,j} \cup \mathcal{A}_{l,j}^{(\text{neighbor})}. \quad (\text{S-15})$$

As will be demonstrated later, if $\mathbf{Q} \cap \hat{\mathcal{A}}_{n,j} = \emptyset$, the basis of the final output state with respect to label j is free of errors.

We consider a specific space-time-polarization configuration of error $c \in \mathcal{P}_{\mathbf{Q}}$ for some $\mathbf{Q} = [Q_1, Q_2, \dots, Q_M]$. We define the set of survived qubits with respect to c as

$$\mathcal{S}_{\text{surv}}(c) \equiv \{q \in V \mid q \notin Q_m \text{ for all } 1 \leq m \leq M\}. \quad (\text{S-16})$$

If a qubit is in $\mathcal{S}_{\text{surv}}(c)$, it means that no error has been applied at it during the algorithm. We then introduce the set of all *good* branch at the l th spatial layer of QRAM as

$$g_l(c) = \{j \mid \mathcal{S}_{\text{surv}}(c) \cap \hat{\mathcal{A}}_{l,j} = \emptyset\}. \quad (\text{S-17})$$

For a lighter notation, we also define

$$\hat{\mathcal{A}}_j \equiv \hat{\mathcal{A}}_{n,j}, \quad (\text{S-18})$$

and

$$g(c) \equiv g_n(c). \quad (\text{S-19})$$

It turns out that the infidelity is closely related to $g(c)$. In below, we discuss the evolution during fanin phase and fanout phase separately.

D. Fanin phase

We assume that before the l th step, the quantum state is in the form of

$$|\tilde{\psi}_{l-1}\rangle = E_{l-1} \sum_{j \in g_{l-1}(c)} \psi_{l-1,j} |\mathcal{B}_{l-1,j}\rangle + |\text{garb}_{l-1}\rangle \quad (\text{S-20})$$

for some unitary E_{l-1} acting trivially in the good branch, and $|\text{garb}_{l-1}\rangle$ orthogonal to the first term. For a lighter notation, in Eq. (S-20), we have neglected the dependency on c , and set $|\tilde{\psi}_{l-1}\rangle \equiv |\tilde{\psi}_{l-1}(c)\rangle$, $E_{l-1} \equiv E_{l-1}(c)$ and $|\text{garb}_{l-1}\rangle = |\text{garb}_{l-1}(c)\rangle$.

For $l = 0$, Eq. (S-20) holds because the initial state $|\mathbf{U}_{0,0}\rangle = |\mathcal{B}_{0,0}\rangle$ is assumed to be error-free. At the l th step, we denote the ideal evolution as $\prod_{j=0}^{2^{l-1}-1} U_{l-1,j}$, with $U_{l-1,j} = \mathbf{R}\mathbf{T}_{l-1,j}\mathbf{C}\mathbf{R}_{l-1,j}$. Note that $U_{l-1,j}$ for different j acts on different qubits and do

not have overlap, so they commute with each other. Moreover, errors act trivially on qubits in good branches. So we can express the unitary at the l th step as

$$\tilde{U}_l = \prod_{j \in g_{l-1}(c)} U_{l,j} \prod_{j \notin g_{l-1}(c)} \tilde{U}_{l,j}. \quad (\text{S-21})$$

For $j \notin g_{l-1}(c)$, the unitary $\tilde{U}_{l,j}$ is the noisy implementation of $U_{l,j}$, which acts trivially at good branches. So the quantum state at the l th step satisfies

$$|\tilde{\psi}_l\rangle = \tilde{U}_l |\tilde{\psi}_{l-1}\rangle \quad (\text{S-22})$$

$$= \tilde{U}_l E_{l-1} \sum_{j \in g_{l-1}} \psi_{l-1,j} |\mathcal{B}_{l-1,j}\rangle + \tilde{U}_l |\text{garb}_{l-1}\rangle \quad (\text{S-23})$$

$$= \left(\prod_{j \notin g_{l-1}(c)} \tilde{U}_{l,j} \right) E_{l-1} \sum_{j \in g_{l-1}(c)} \tilde{U}_{l,j} \psi_{l-1,j} |\mathcal{B}_{l-1,j}\rangle + \tilde{U}_l |\text{garb}_{l-1}\rangle \quad (\text{S-24})$$

$$= E_l \sum_{\lfloor j/2 \rfloor \in g_{l-1}(c)} \psi_{l,j} |\mathcal{B}_{l,j}\rangle + \tilde{U}_l |\text{garb}_{l-1}\rangle \quad (\text{S-25})$$

$$= E_l \sum_{j \in g_l(c)} \psi_{l,j} |\mathcal{B}_{l,j}\rangle + |\text{garb}_l\rangle. \quad (\text{S-26})$$

In Eq. (S-25), we have defined $E_l \equiv (\prod_{j \notin g_{l-1}(c)} \tilde{U}_{l,j}) E_{l-1}$; in Eq. (S-26), we have defined

$$|\text{garb}_l\rangle = E_l \sum_{j \in \{j' | \lfloor j'/2 \rfloor \in g_{l-1}(c) \& j' \notin g_l(c)\}} \psi_{l,j} |\mathcal{B}_{l,j}\rangle + U_l^{\text{enc}} |\text{garb}_{l-1}\rangle.$$

Accordingly, the final state of the encoding phase is in the form of

$$|\tilde{\psi}_n\rangle = \sum_{j \in g(c)} \psi_j E |\mathcal{B}_j\rangle + |\text{garb}\rangle, \quad (\text{S-27})$$

where $E \equiv E_n$, $\mathcal{B}_j = \mathcal{B}_{n,j}$, and $|\text{garb}\rangle \equiv |\text{garb}_n\rangle$. Note that unitary E acts trivially at qubits in good branches, and $|\text{garb}\rangle$ is orthogonal to the first term.

E. Fanout phase

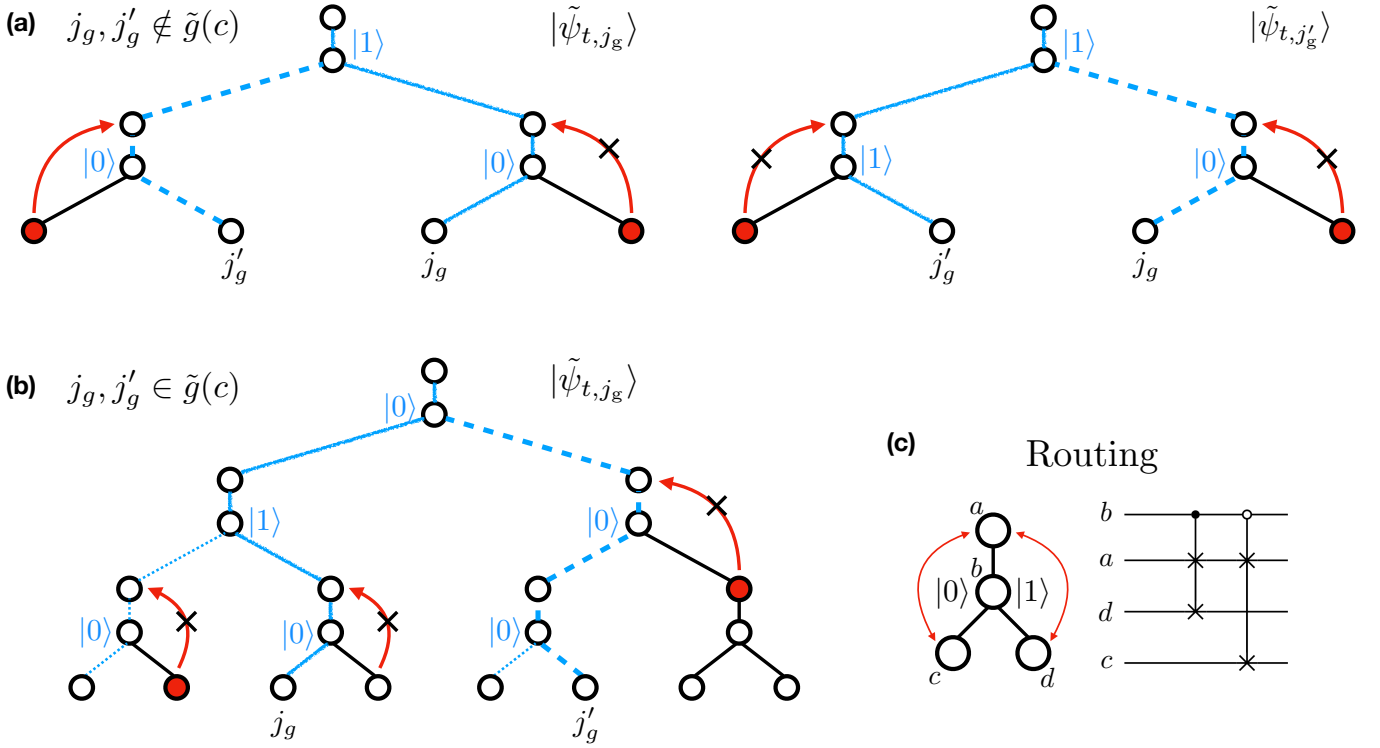
We then study the fanout phase. Our discussion mainly follows the ideal in Sec.V of [25]. In the fanout phase, all operations (under a specific error configuration c) only transfer a computational basis to another computational basis, up to a phase. So we can always express the quantum state before the t th step as

$$|\tilde{\psi}_t'\rangle = \sum_{j \in g(c)} \psi_j |\psi'_{t,j}\rangle + |\text{garb}'_t\rangle, \quad (\text{S-28})$$

where $|\psi'_{t,j}\rangle$ is some computational basis up to a phase, and $|\text{garb}'_t\rangle$ is orthogonal to the first term. Similar to the encoding phase, the expression of states neglect the dependency on c . For $t = 0$, Eq. (S-28) corresponds to $|\psi'_{0,j}\rangle = E |\mathcal{B}_j\rangle$ and $|\text{garb}'_0\rangle = |\text{garb}\rangle$.

At each step, we suppose a routing operation $\mathbf{RT}_{l',j'}$ acts nontrivially at a good branch $j \in g(c)$ (this also indicates that it is error-free). It can be verified that $\mathbf{RT}_{l',j'}$ only swaps $\mathbf{U}_{l,j}$ and one of the children qubit of $\mathbf{D}_{l,j}$ that is within the branch j , while another child qubit of $\mathbf{D}_{l,j}$ remains unchanged (see Fig. S1(a)). Moreover, swap gates in the good branch is also error-free. Applying this argument on each elementary routing and swapping operations, the fanout phase performs the basis transformation $E |\mathcal{B}_j\rangle \rightarrow |f_j\rangle_{\text{qram}} \otimes |j\rangle_{\text{out}}$ for all $j \in g(c)$. Here, $|f_j\rangle_{\text{qram}} \equiv |f_j(c)\rangle_{\text{qram}}$ is some quantum state of the QRAM. Accordingly, the final state of the fanout phase, $|\tilde{\psi}'\rangle \equiv |\tilde{\psi}'_{t_{\text{end}}}\rangle$ with t_{end} the last step, is in the form of

$$|\tilde{\psi}'\rangle = \sum_{j \in g(c)} \psi_j |f_j\rangle_{\text{qram}} \otimes |j\rangle_{\text{out}} + |\text{garb}'\rangle, \quad (\text{S-29})$$



Supplementary Figure S1: (a) For $j_g, j'_g \in g(c)$ but $j_g, j'_g \notin \tilde{g}(c)$, errors may propagate upward into the good branch from the left hand side. In particular, at the left figure for basis $|\tilde{\psi}_{t,j_g}\rangle$, error propagate into the branch j'_g . (b) For basis $|\psi_{t,j_g}\rangle$, routing qubits at all good branches $j'_g \neq j_g$ are always at state $|0\rangle$. With this property, error will never propagate into branches in $\tilde{g}(c)$. (c) Sketch of the routing operations.

for some $|garb'\rangle$ orthogonal to the first term.

However, Eq. (S-67) is still not sufficient for us to estimate the infidelity. For $j, j' \in g(c)$, we in general have $|f_j\rangle_{\text{qram}} \neq |f_{j'}\rangle_{\text{qram}}$ when $j \neq j'$. After tracing out the QRAM part of Eq. (S-67), the coherence between basis in $g(c)$ may be destroyed. To understand why $|f_j\rangle_{\text{qram}} \neq |f_{j'}\rangle_{\text{qram}}$ (see also Sec.V of [25]), we should analyze how error terms propagate from different branches. We first consider basis $|\psi_{t,j_g}\rangle$ with $j_g \in g(\mathcal{Q})$. As shown in left subfigure of Fig. S1 (a), suppose an error occurs at the bad branch $j_b \notin g(\mathcal{Q})$, it may propagate into another good branch $j'_g \in g(\mathcal{Q})$ ($j'_g \neq j_g$) through a sequence of routing operations (Fig. S1(c)). On the other hand, if we consider the basis $|\psi_{t,j'_g}\rangle$ instead, errors will never propagate into j'_g (see also right subfigure of Fig. S1). So in general the final state of the QRAM is different for different basis in $g(c)$.

Fortunately, we can identify a large portion of basis in Eq. (S-67), such that errors will still *not* propagate from bad branches to any of the good branches. For these j , the final states of QRAM, $|f_j\rangle_{\text{qram}}$, is independent of j . To begin with, we notices that in every good branches, error only propagate into it from the right hand side (instead of left hand side). The reason is as follows. Let us consider a basis $|\psi_{t,j_g}\rangle$ with $j_g \in g(c)$. For branch j_g , errors will not propagate into it as mentioned previously. For another good branch $j'_g \neq j_g$, all routing qubits in it (those in lower sublayers) is at the default state $|0\rangle$. Therefore, swap is only performed between its parent and its right child.

With the argument above, we suppose $k_1 k_2 \cdots k_l 0 \cdots 0$ is a good branch, then no errors will ever propagate upward through $\mathbf{RT}_{l-1,k}$ (with $k = k_1 k_2 \cdots k_l$). Therefore, for index j , if we have $j_1 j_2 \cdots j_l 0 \cdots 0 \in g(c)$ for all $0 \leq l \leq n-1$, no error will propagate into the branch j from any site. Accordingly, we can define the set of all *error-free* branches

$$g'(c) \equiv \{j \in g(c) | \tilde{j}_l \in g(c) \text{ for } 0 \leq l \leq n-1\} \quad (\text{S-30})$$

where

$$\tilde{j}_l \equiv j_1 j_2 \cdots j_l \underbrace{0 \cdots 0}_{n-l}. \quad (\text{S-31})$$

For the basis $|f_j\rangle_{\text{qram}} \otimes |j\rangle$ of the final state, if $j \in g'(c)$, errors are only applied at good branches. So for all $j \in g'(c)$, their

QRAM part is identical, i.e. $|f_j\rangle = |f\rangle$ for some quantum state $|f\rangle$. Then, Eq. (S-67) can be rewritten as

$$|\tilde{\psi}'\rangle = \sum_{j \in g'(c)} \psi_j |f\rangle_{\text{qram}} \otimes |j\rangle_{\text{out}} + |\widetilde{\text{garb}}'\rangle. \quad (\text{S-32})$$

Note that $|f\rangle$ is independent of j , but still depends on c .

F. State preparation infidelity

In Sec. IE, the final output state is $|\tilde{\psi}'\rangle$. Comparing Eq. (S-32) to Eq. (S-11), we have

$$\tilde{\rho}_{\text{out}}(c) = \text{Tr}_{\text{qram}} [|\tilde{\psi}'\rangle\langle\tilde{\psi}'|]. \quad (\text{S-33})$$

We define $|\psi'\rangle \equiv \sum_{j=1}^{N-1} \psi_j |f\rangle_{\text{qram}} \otimes |j\rangle_{\text{out}}$. The fidelity between $|\psi'\rangle$ and Eq. (S-32) is

$$\text{Fid}(|\psi'\rangle\langle\psi'|, |\tilde{\psi}'\rangle\langle\tilde{\psi}'|) = \sum_{j \in g'(c)} |\psi_j|^2 \equiv \Lambda'(c). \quad (\text{S-34})$$

Here, $\Lambda'(c)$ highlights that it depends on c . Because fidelity is non-decreasing under partial trace, we have

$$\text{Fid}(\text{Tr}_{\text{qram}} [|\psi'\rangle\langle\psi'|], \tilde{\rho}(c)) \geq \Lambda'(c). \quad (\text{S-35})$$

Moreover, it can be verified that $\text{Tr}_{\text{qram}} [|\psi'\rangle\langle\psi'|] = \rho_{\text{id}}$. So

$$\text{Fid}(\rho_{\text{id}}, \tilde{\rho}(c)) \geq \Lambda'(c). \quad (\text{S-36})$$

Combining with Eq. (S-12), the total state preparation infidelity satisfies

$$F \geq \mathbb{E}[\Lambda'(c)], \quad (\text{S-37})$$

where $\mathbb{E}[\Lambda'(c)]$ represents the expectation value of $\Lambda(c)$ when sampling c according to p_c .

We now estimate $\mathbb{E}[\Lambda'(c)]$. Let $\mathcal{J} = \{0, 1, \dots, N-1\}$ be all indexes, and $\text{Power}(\mathcal{J})$ be the set of all subset of \mathcal{J} . By definition, we have

$$\mathbb{E}[\Lambda'(c)] = \sum_{J \in \text{Power}(\mathcal{J})} \sum_{j \in J} |\psi_j|^2 \times \Pr[J_1 \in g'(c)] \Pr[J_2 \in g'(c) | J_1 \in g'(c)] \Pr[J_3 \in g'(c) | J_1, J_2 \in g'(c)] \cdots. \quad (\text{S-38})$$

In Eq. (S-38), J_1, J_2, \dots are elements of J arranged in arbitrary order. Note that different branches may have overlap, and we always have

$$\Pr[J_2 \in g'(c) | J_1 \in g'(c)] \geq \Pr[J_2 \in g'(c)], \quad (\text{S-39})$$

$$\Pr[J_3 \in g'(c) | J_1, J_2 \in g'(c)] \geq \Pr[J_3 \in g'(c)], \quad (\text{S-40})$$

and so on. Therefore, we have

$$\mathbb{E}[\Lambda'(c)] \geq \sum_{J \in \text{Power}(\mathcal{J})} \sum_{j \in J} |\psi_j|^2 \times \Pr[J_1 \in g'(c)] \Pr[J_2 \in g'(c)] \Pr[J_3 \in g'(c)] \cdots \quad (\text{S-41})$$

$$= \sum_{j=0}^{N-1} |\psi_j|^2 \Pr[j \in g'(c)] \quad (\text{S-42})$$

$$= \Pr[j \in g'(c)] \quad (\text{S-43})$$

Eq. (S-42) is because the right hand side of Eq. (S-41) corresponds to a summation of multiple variables sampled independently. Eq. (S-43) is because of the normalization of ψ_j , and the probability is independent of j . By definition in Eq. (S-30), j is an error-free branch in $g'(c)$, if and only if all qubits in \tilde{j}_l (for all $0 \leq l \leq n-1$) are free of error at all time. There are at most $O(n^2)$ of these qubits. For each individual qubit, the probability that it is error free at all time is $(1 - \varepsilon)^{O(n)}$, because the algorithm has totally $O(n)$ steps. Therefore, with probability $((1 - \varepsilon)^{O(n)})^{O(n^2)} = (1 - \varepsilon)^{O(n^3)}$, j is a good branch. By Bernoulli inequality,

we have $\Pr[j \in g'(c)] \geq 1 - A\epsilon n^3$ for some constant A . So we have

$$\mathbb{E}[\Lambda'(c)] \geq (1 - A\epsilon n^3). \quad (\text{S-44})$$

Combining with Eq. (S-37), we have

$$1 - F \leq A\epsilon n^3. \quad (\text{S-45})$$

II. 3-QUBIT-PER-NODE PROTOCOL

A. Hardware architecture and basic operations

In our 3-qubit-per-node protocol, each layer contains 3 sublayers. The upper, middle, and lower sublayers of the l th layer are denoted as (l, \uparrow) , (l, \bullet) , and (l, \downarrow) respectively. Each sublayer contain 2^l qubits, each denoted as $\mathbf{U}_{l,j}$, $\mathbf{M}_{l,j}$, $\mathbf{D}_{l,j}$ respectively with $0 \leq j \leq 2^l - 1$. The children of $\mathbf{U}_{l,j}$, $\mathbf{M}_{l,j}$ and $\mathbf{D}_{l,j}$ are $\{\mathbf{M}_{l,j}\}$, $\{\mathbf{D}_{l,j}\}$, and $\{\mathbf{U}_{l+1,2j}, \mathbf{U}_{l+1,2j+1}\}$ respectively. Moreover, the output register is identical to the 2-qubit-per-node protocol. The hardware architecture contains more qubits (totally $6N - 3$ qubits), but each qubit is still connected to at most 3 other qubits.

We then introduce some basic operations. Let $r_{l,j} \equiv \begin{pmatrix} \psi_{l+1,2j}/\psi_{l,j} & * \\ \psi_{l+1,2j+1}/\psi_{l,j} & \diamond \end{pmatrix}$, where $*$ and \diamond are some complex values that make $r_{l,j}$ be a unitary. We have the following basic operations.

- $\mathbf{R}_{l,j}$: rotation $r_{l,j}$ applied at qubit $\mathbf{D}_{l,j}$
- $\overline{\mathbf{CR}}_{l,j}$: controlled rotation $|0\rangle\langle 0| \otimes r_{l,j}^\dagger + |1\rangle\langle 1| \otimes \mathbb{I}$ with $\mathbf{M}_{l,j}$ and $\mathbf{D}_{l,j}$ as controlled and target qubits
- $\mathbf{CNOT}_{l,j}$: CNOT gate with $\mathbf{U}_{l,j}$ and $\mathbf{M}_{l,j}$ be the control and target qubits
- $\mathbf{CRT}_{l,j}$: Five-qubit-gate

$$|0\rangle_{\mathbf{M}_{l,j}}\langle 0| \otimes \mathbb{I} + |1\rangle_{\mathbf{M}_{l,j}}\langle 1| \otimes |0\rangle_{\mathbf{D}_{l,j}}\langle 0| \otimes \mathbf{S}(\mathbf{U}_{l,j}, \mathbf{U}_{l+1,2j}) + |1\rangle_{\mathbf{M}_{l,j}}\langle 1| \otimes |1\rangle_{\mathbf{D}_{l,j}}\langle 1| \otimes \mathbf{S}(\mathbf{U}_{l,j}, \mathbf{U}_{l+1,2j+1})$$

- $\mathbf{S}_{l,j}^{(\uparrow, \bullet)}$: swap gate between $\mathbf{U}_{l,j}, \mathbf{M}_{l,j}$
- $\mathbf{S}_{l,j}^{(\uparrow, \downarrow)}$: swap gate between $\mathbf{U}_{l,j}, \mathbf{D}_{l,j}$

Accordingly, we define the following parallel operations

$$\mathbf{PR} \equiv \sum_{l=0}^{n-1} \sum_{j=0}^{2^l-1} \mathbf{R}_{l,j}, \quad \overline{\mathbf{PCR}} \equiv \sum_{l=0}^{n-1} \sum_{j=0}^{2^l-1} \overline{\mathbf{CR}}_{l,j} \quad (\text{S-46})$$

that applies at all l, j , and

$$\mathbf{PCNOT}_l \equiv \sum_{j=0}^{2^l-1} \mathbf{R}_{l,j}, \quad \mathbf{PCRT}_l \equiv \sum_{j=0}^{2^l-1} \mathbf{R}_{l,j}, \quad \mathbf{PS}_l^{(\uparrow, \bullet)} \equiv \sum_{j=0}^{2^l-1} \mathbf{S}_{l,j}^{(\uparrow, \bullet)}, \quad \mathbf{PS}_l^{(\uparrow, \downarrow)} \equiv \sum_{j=0}^{2^l-1} \mathbf{S}_{l,j}^{(\uparrow, \downarrow)} \quad (\text{S-47})$$

that act on a specific layer $0 \leq l \leq n$. All parallel operations above can be implemented with $O(1)$ layer of single- and two-qubit gates.

B. Fanin phase

The pseudo code of our algorithm is illustrated in Algorithm. S1 and Algorithm. S2. Our method is inspired by the pre-rotation technique in [13], which encodes angles $\{\psi_{l,j}\}$ before the controlled routing. The advantage is that pre-rotation can push the Clifford+ T depth to a linear scaling. For clarity, we discuss the single- and two-qubit decomposition in this section, while the Clifford+ T decomposition will be introduced in Sec. III E.

Let $\mathcal{D} = \{\mathbf{D}_{l,j} | 0 \leq l \leq n-1, 0 \leq j \leq 2^l - 1\}$ be the set of all qubits in the lower sublayers. We first implement parallel rotation **PR**, and \mathcal{D} is prepared as

$$|\theta\rangle_{\mathcal{D}} \equiv \bigotimes_{\mathbf{D}_{l,j} \in \mathcal{D}} \left(\psi_{l+1,2j} / \psi_{l,j} |0\rangle_{\mathbf{D}_{l,j}} + \psi_{l+1,2j+1} / \psi_{l,j} |1\rangle_{\mathbf{D}_{l,j}} \right). \quad (\text{S-48})$$

Qubits in \mathcal{D} serves as the routing qubits of our subsequent controlled-routing operations.

Let $\mathcal{A}_{l,\downarrow,j}$ be all ancestors of $\mathbf{D}_{l,j}$ at lower sublayers, and we further define $\overline{\mathcal{D}}_{l,j} = \mathcal{D} - \mathcal{A}_{l,\downarrow,j}$. $\mathcal{D}_{l,j}$ represents all routing qubits in \mathcal{D} that are irrelevant to the operation **CRT** $_{l,j}$ during our fanin process. We also define

$$|\theta\rangle_{\mathcal{D}_{l,j}} \equiv \bigotimes_{\mathbf{D}_{l',j'} \in \mathcal{D}_{l,j}} \left(\psi_{l'+1,2j'} / \psi_{l',j'} |0\rangle_{\mathbf{D}_{l',j'}} + \psi_{l'+1,2j'+1} / \psi_{l',j'} |1\rangle_{\mathbf{D}_{l',j'}} \right) \quad (\text{S-49})$$

as the quantum state of the subsystem $\mathcal{D}_{l,j}$ for Eq. (S-48). Let $\mathcal{M}_{l,j} \equiv \{\mathbf{M}_{0,0}\} \cup \{\mathbf{M}_{l',j:l'} | 1 \leq l' \leq l-1\}$, and $\mathcal{C}_{l,j} \equiv \mathcal{M}_{l,j} \cup \mathcal{B}_{l,j}$ (with $\mathcal{B}_{l,j}$ defined in Eq. (4)), we will then iteratively perform the transformation

$$|\psi_l\rangle \rightarrow |\psi_{l+1}\rangle, \quad (\text{S-50})$$

where

$$|\psi_l\rangle = \sum_{j=0}^{2^l-1} \psi_{l,j} |\theta\rangle_{\mathcal{D}_{l,j}} \otimes |\mathcal{C}_{l,j}\rangle_{\mathcal{V}-\mathcal{D}_{l,j}}. \quad (\text{S-51})$$

Note that $|\psi_0\rangle = |\theta\rangle_{\mathcal{D}} \otimes |\{\mathbf{D}_{0,0}\}\rangle$. In Eq. (S-51), quantum state of qubit set $\mathcal{D}_{l,j}$ and $\mathcal{V} - \mathcal{D}_{l,j}$ (all qubits not in $\mathcal{D}_{l,j}$) are expressed in the form of computational basis representation and activation representation, respectively.

By implementing parallel CNOT gates, we have **PCNOT** $_l |\mathcal{C}_{l,j}\rangle_{\mathcal{V}-\mathcal{D}_{l,j}} = |\mathcal{C}_{l,j} \cup \{\mathbf{M}_{l,j}\}\rangle_{\mathcal{V}-\mathcal{D}_{l,j}}$, and hence

$$\mathbf{PCNOT}_l |\psi_l\rangle = \sum_{j=0}^{2^l-1} \psi_{l,j} |\theta\rangle_{\mathcal{D}_{l,j}} \otimes |\mathcal{C}_{l,j} \cup \{\mathbf{M}_{l,j}\}\rangle_{\mathcal{V}-\mathcal{D}_{l,j}}. \quad (\text{S-52})$$

Then, if we apply **CRT** $_{l,j}$ on Eq. (S-52), only basis with label j will be changed. This is because the routing is controlled on $\mathbf{M}_{l,j}$. We notice that the basis with label j can be rewritten as

$$\psi_{l,j} \left(|\theta\rangle_{\mathcal{D}_{l,j}} \otimes |\mathcal{C}_{l,j} \cup \{\mathbf{M}_{l,j}\}\rangle_{\mathcal{V}-\mathcal{D}_{l,j}} \right) \quad (\text{S-53})$$

$$= \psi_{l,j} |\theta\rangle_{\mathcal{D}_{l,j}-\{\mathbf{D}_{l,j}\}} \otimes \left(\psi_{l+1,2j} / \psi_{l,j} |\mathcal{C}_{l,j} \cup \{\mathbf{M}_{l,j}\}\rangle_{\mathcal{V}-\mathcal{D}_{l,j}-\{\mathbf{D}_{l,j}\}} + \psi_{l+1,2j+1} / \psi_{l,j} |\mathcal{C}_{l,j} \cup \{\mathbf{M}_{l,j}, \mathbf{D}_{l,j}\}\rangle_{\mathcal{V}-\mathcal{D}_{l,j}-\{\mathbf{D}_{l,j}\}} \right) \quad (\text{S-54})$$

$$= \psi_{l+1,2j} |\theta\rangle_{\mathcal{D}_{l+1,2j}} \otimes |\mathcal{C}_{l,j} \cup \{\mathbf{M}_{l,j}\}\rangle_{\mathcal{V}-\mathcal{D}_{l+1,2j}} + \psi_{l+1,2j+1} |\varphi\rangle_{\mathcal{D}_{l+1,2j+1}} \otimes |\mathcal{C}_{l,j} \cup \{\mathbf{M}_{l,j}, \mathbf{D}_{l,j}\}\rangle_{\mathcal{V}-\mathcal{D}_{l+1,2j+1}}. \quad (\text{S-55})$$

It can be verified that

$$\mathbf{CRT}_{l,j} |\mathcal{C}_{l,j} \cup \{\mathbf{M}_{l,j}\}\rangle_{\mathcal{V}-\mathcal{D}_{l+1,2j}} = |\mathcal{C}_{l+1,2j}\rangle_{\mathcal{V}-\mathcal{D}_{l+1,2j}} \quad (\text{S-56})$$

$$\mathbf{CRT}_{l,j} |\mathcal{C}_{l,j} \cup \{\mathbf{M}_{l,j}, \mathbf{U}_{l,j}\}\rangle_{\mathcal{V}-\mathcal{D}_{l+1,2j+1}} = |\mathcal{C}_{l+1,2j}\rangle_{\mathcal{V}-\mathcal{D}_{l+1,2j+1}}. \quad (\text{S-57})$$

Therefore, we have

$$\begin{aligned} \mathbf{PCRT}_l \mathbf{PCNOT}_l |\psi_l\rangle &= \sum_{j=0}^{2^l-1} \psi_{l+1,2j} |\theta\rangle_{\mathcal{D}_{l+1,2j}} \otimes |\mathcal{C}_{l+1,2j}\rangle_{\mathcal{V}-\mathcal{D}_{l+1,2j}} + \psi_{l+1,2j+1} |\theta\rangle_{\mathcal{D}_{l+1,2j+1}} \otimes |\mathcal{C}_{l+1,2j+1}\rangle_{\mathcal{V}-\mathcal{D}_{l+1,2j+1}} \\ &= \sum_{j=0}^{2^{l+1}-1} \psi_{l,j} |\theta\rangle_{\mathcal{D}_{l,j}} \otimes |\mathcal{C}_{l,j}\rangle_{\mathcal{V}-\mathcal{D}_{l,j}} \\ &= |\psi_{l+1}\rangle. \end{aligned} \quad (\text{S-58})$$

Applying $\mathbf{PCRT}_l/\mathbf{PCNOT}_l$ iteratively from $l = 0$ to $l = n - 1$, we obtain

$$|\psi_n\rangle = \sum_{j=0}^{N-1} \psi_j |\theta\rangle_{\mathcal{D}_{n,j}} \otimes |\mathcal{E}_{n,j}\rangle_{\mathcal{V}-\mathcal{D}_{n,j}}. \quad (\text{S-59})$$

In the last step, we perform $\overline{\mathbf{PCR}}$, which performs of $r_{l,j}^\dagger$ on $\mathbf{D}_{l,j}$ conditioned on $\mathbf{M}_{l,j}$ not activated. For basis with label j , at the middle sublayers, only qubits $\mathbf{M}_{n-1,j}$, $\mathbf{M}_{n-2,j_{1:n-1}}$, \dots , \mathbf{M}_{0,j_1} are activated. These qubits are not in $\mathcal{D}_{n,j}$, so $|\theta\rangle_{\mathcal{D}_{n,j}}$ are uncomputed, and the final state is

$$|\psi\rangle = \overline{\mathbf{PCR}}|\psi_n\rangle = \sum_{j=0}^{N-1} \psi_j |\mathcal{E}_{n,j}\rangle_{\mathcal{V}}. \quad (\text{S-60})$$

Eq. (S-60) is similar to the one for 2-qubit-per-node protocol. The only difference is that for basis j , all ancestors of $\mathbf{U}_{n,j}$ in sublayers (l, \bullet) are activated. In the next section, with a mild modification of the fanout phase, we can uncompute the QRAM while obtain the target state in the output register.

C. Fanout phase

Let

$$\mathcal{E}'_{l,j} = \mathcal{M}_{l,j} \cup \mathcal{B}'_{l,j}, \quad (\text{S-61})$$

with $\mathcal{B}'_{l,j}$ defined in Eq. (4), it can be verified that

$$\mathbf{NOT}(\mathbf{U}_{0,0})\mathbf{PCRT}_1\mathbf{PCRT}_2 \cdots \mathbf{PCRT}_{n-1}|\mathcal{E}_{n,j}\rangle = |\mathcal{E}'_{n,j}\rangle. \quad (\text{S-62})$$

In other words, performing parallel controlled routing from $l = n - 1$ to $l = 0$ transfers the excitation at layer (n, \uparrow) to $\mathbf{U}_{0,0}$, which can be uncomputed by an extra not gate. Our strategy is to perform the following transformation

$$|\mathcal{E}'_{l,j_{1:l}}\rangle \otimes |0 \cdots 0_{j_{l+1}} \cdots j_n\rangle_{\text{out}} \longrightarrow |\mathcal{E}'_{l,j_{1:l-1}}\rangle \otimes |0 \cdots 0_{j_l} \cdots j_n\rangle_{\text{out}}. \quad (\text{S-63})$$

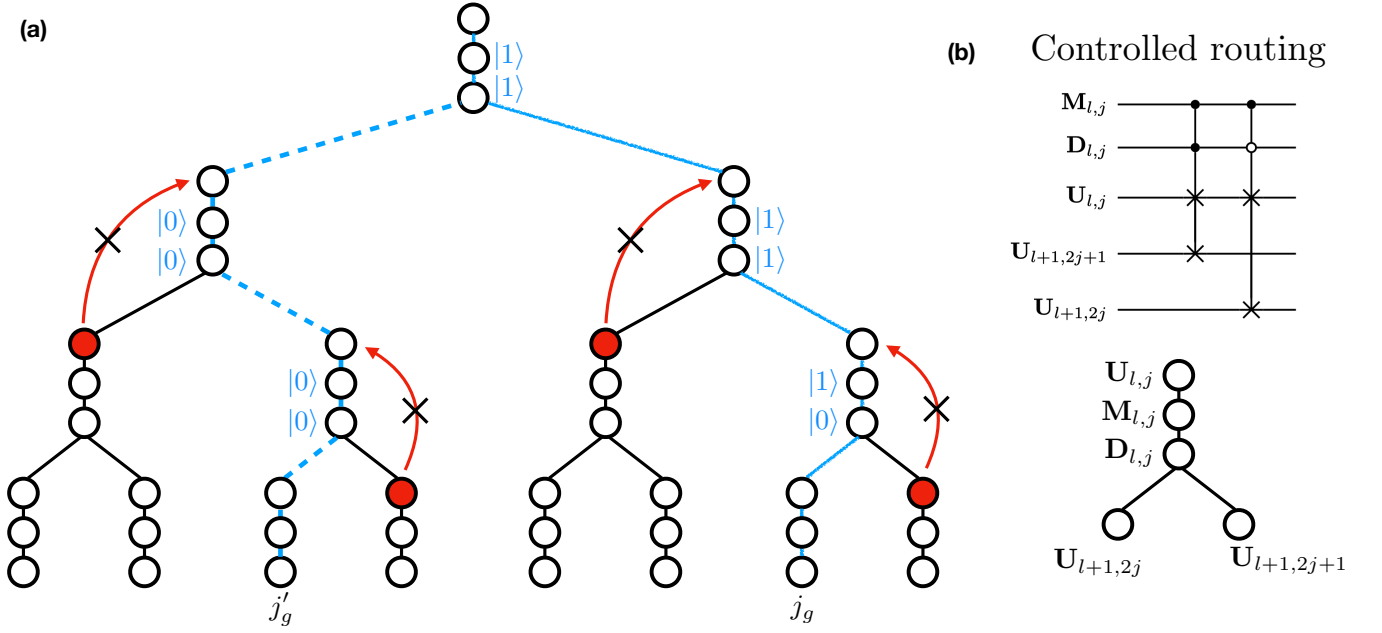
iteratively. For basis $|\mathcal{E}'_{l,j_{1:l}}\rangle$, we can also deterministically route the activation at layer (l, \bullet) to $\mathbf{U}_{0,0}$, and uncompute it with a NOT gate, i.e.

$$\mathbf{NOT}(\mathbf{U}_{0,0})\mathbf{PCRT}_1\mathbf{PCRT}_2 \cdots \mathbf{PCRT}_{l-1}\mathbf{PS}_l^{(\uparrow, \bullet)}|\mathcal{E}'_{l,j_{1:l}}\rangle = |\mathcal{E}'_{l,j_{1:l}} - \{\mathbf{M}_{l,j_{1:l}}\}\rangle. \quad (\text{S-64})$$

Moreover, in analogy to the 2-qubit-per-node protocol, we can route the state $|j_l\rangle$ from layer (l, \downarrow) to qubit \mathbf{O}_l in the output register.

$$\begin{aligned} & \mathbf{S}(\mathbf{U}_{0,0}, \mathbf{O}_l)\mathbf{PCRT}_1\mathbf{PCRT}_2 \cdots \mathbf{PCRT}_{l-1}\mathbf{PS}_l^{(\uparrow, \downarrow)}|\mathcal{E}'_{l,j_{1:l}} - \{\mathbf{M}_{l,j_{1:l}}\}\rangle \otimes |0 \cdots 0_{j_{l+1}} \cdots j_n\rangle_{\text{out}} \\ & = |\mathcal{E}'_{l,j_{1:l-1}}\rangle \otimes |0 \cdots 0_{j_l} \cdots j_n\rangle_{\text{out}}. \end{aligned} \quad (\text{S-65})$$

We can start the operation in Eq. (S-65) after the operation in Eq. (S-64) has finished the \mathbf{PCRT}_{l-2} , and two operations will not affect each other. With an abuse of notation, we also define this process as $\mathbf{Fanout}(l - 1)$ (for $1 \leq l \leq n$), which performs the transformation claimed in Eq. (S-63). We also define $\mathbf{Fanout}(n)$ as the process corresponding to Eq. (S-62). By implementing $\mathbf{Fanout}(n)$, $\mathbf{Fanout}(n - 1)$, \dots , $\mathbf{Fanout}(0)$ iteratively, we can uncompute the QRAM, while prepare the target state at output register. Similar to the 2-site-per-node protocol, while implementing $\mathbf{Fanout}(l)$ sequentially is time costly, we can start another before one finished. More specifically, we can start $\mathbf{Fanout}(l)$, idle for 5 steps, and then start $\mathbf{Fanout}(l - 1)$. In this way, operations $\mathbf{Fanout}(l)$ and $\mathbf{Fanout}(l - 1)$ will not affect each other, and the total runtimes is $O(n)$.



Supplementary Figure S2: (a) For both $j_g \in g(c)$ and $j'_g \in g(c)$, errors never propagate into the good branches (blue color), because all controlled qubits $M_{l,j}$ in good branches are error free. (c) Sketch of the controlled routing operations.

Algorithm S1 Quantum state preparation. Initial state $|U_{0,1}\rangle$, amplitudes $\{\psi_{l,j}\}$ as input

```

implement PR
for  $l = 0, \dots, n-1$ :
  implement PCNOT $_l$ 
  implement PCRT $_l$ 
implement PCR
for  $m = 0$  to  $n$ :
  start Fanout( $n-m$ )
  idle for 6 steps

```

Algorithm S2 Subroutine Fanout(l) for 3-qubit-per-node scheme

```

if  $l \neq n$ :
  for  $l' = 1$  to  $l' = l$ 
    implement PRT $_{l-l'}$  # takes 1 steps
else if  $l \neq n$ :
  implement PS $_l^{(\uparrow, \bullet)}$  # takes 1 step
  implement PRT $_{l-2}$ PRT $_{l-1}$  # takes 2 steps
  implement PS $_l^{(\uparrow, \downarrow)}$  # takes 2 step
  for  $l' = 1$  to  $l' = l-2$ 
    implement PRT $_{l-l'}$ PRT $_{l-l'-2}$  # takes 1 steps
  NOT( $U_{0,1}$ ) # takes 1 steps
  implement PRT $_0$ PRT $_1$  # takes 2 steps
  S( $U_{0,1}, O_l$ ) # takes  $l$  steps

```

D. Robustness analysis

With an abuse of notation, we define *good* index and relevant terminologies here in a similar way to the 2-qubit-per-node protocol. Let \mathcal{A}_j be all ancestors of $U_{n,j}$ in both QRAM and output register. We also define $\hat{\mathcal{A}}_j$ as the intersection of \mathcal{A}_j and its

nearest neighbour. Similar to the 2-qubit-per-node protocol, for a specific space-time-polarization configuration of error c , we define $g(c)$ as set of all *good* index j , such that all qubits in \mathcal{A}_j are free of errors at all time.

With the same argument to the 2-qubit-per-node protocol, the final output state of can be expressed as

$$|\tilde{\psi}'\rangle = \sum_{j \in g(c)} \psi_j |f_j\rangle_{\text{qram}} \otimes |j\rangle_{\text{out}} + |\text{garb}'\rangle \quad (\text{S-66})$$

for some garbage state that is orthogonal to the first term. Yet, the main difference is that in the 3-qubit-per-node protocol here, errors will never propagate into the good branches $j \in g(c)$ (as oppose to $j \in g'(c)$ in the 2-qubit-per-node protocol). The reason is as follows (see also Fig. S2). During the fanout process, we suppose the quantum state at a certain step t is

$$|\tilde{\psi}'_t\rangle = \sum_{j \in g(c)} \psi_j |\psi'_{t,j}\rangle_{\text{out}} + |\text{garb}'_t\rangle. \quad (\text{S-67})$$

We now consider basis $|\psi'_{t,j_b}\rangle$ for some $j_g \in g(c)$. During controlled routing operations, errors will not propagate into the branch j_g , because the controlled and routing qubits are at correct state. We now consider other good branch $j'_g \in g(c)$ that $j'_g \neq j_g$. All of their control qubits in the middle sublayers are free of errors, and hence at state $|0\rangle$. Therefore, all corresponding routing operations does not perform any swapping, and errors will not propagate from bad branch to the branch j'_g .

As a result, errors perform trivially at all good branches, so for all $j \in g(c)$, we have $|f_j\rangle_{\text{qram}} = |f\rangle_{\text{qram}}$ for some computational basis f independent of j . Let $\Lambda = \sum_{j \in g(c)} |\psi_j|^2$, with the same argument for obtaining Eq. (S-37) in Sec. IF, we have $F \geq \mathbb{E}[\Lambda]$. Similar to Eq. (S-43), we also have

$$\mathbb{E}[\Lambda] \geq \Pr[j \in g(c)]. \quad (\text{S-68})$$

Because $\mathcal{A}_j = O(n)$ and the algorithm has runtime $O(n)$, we have $\Pr[j \in g(c)] \geq (1 - \varepsilon)^{O(n) \times O(n)} \geq 1 - A\varepsilon n^2$ for some constant A . Therefore, the total infidelity satisfies

$$1 - F \leq A\varepsilon n^2. \quad (\text{S-69})$$

E. Clifford+ T decomposition

1. Decomposition protocol and error analysis

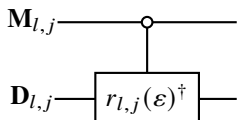
Among all elementary single- and two-qubit gates, only rotations $\mathbf{R}_{l,j}$ and controlled rotations $\overline{\mathbf{C}}\mathbf{R}_{l,j}$ has decomposition error, while all other elementary gates can be ideally constructed with constant number of Clifford and T gates.

According to [49], given an arbitrary z-rotation $R_z(\alpha)$ and accuracy $\varepsilon > 0$, we can always construct a single qubit rotation $R_z(\alpha, \varepsilon)$ with $O(\log(1/\varepsilon))$ depth of H and T gates, such that $\|R_z(\alpha, \varepsilon) - R_z(\alpha)\| \leq \varepsilon$. For y-rotation $R_y(\beta)$, the result is similar. Moreover, we can always decompose each $r_{l,j}$ into the concatenation of a y-rotation and a z-rotation $r_{l,j} = R_z(\alpha_{l,j})R_y(\beta_{l,j})$. We approximate $\mathbf{R}_{l,j}$ with the following quantum circuit

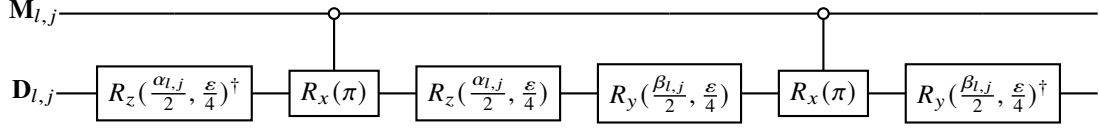
$$\mathbf{R}_{l,j}(\varepsilon) \equiv \mathbf{D}_{l,j} \text{---} \boxed{r_{l,j}(\varepsilon)} \text{---} \equiv$$

$$\mathbf{D}_{l,j} \text{---} \boxed{R_y\left(\frac{\beta_{l,j}}{2}, \frac{\varepsilon}{4}\right)} \text{---} \boxed{R_x(\pi)} \text{---} \boxed{R_y\left(\frac{\beta_{l,j}}{2}, \frac{\varepsilon}{4}\right)^\dagger} \text{---} \boxed{R_z\left(\frac{\alpha_{l,j}}{2}, \frac{\varepsilon}{4}\right)^\dagger} \text{---} \boxed{R_x(\pi)} \text{---} \boxed{R_z\left(\frac{\alpha_{l,j}}{2}, \frac{\varepsilon}{4}\right)} \text{---}$$

Note that $R_z\left(\frac{\alpha_{l,j}}{2}, \frac{\varepsilon}{4}\right)^\dagger$ can be constructed by inverse the H, T gate sequence of $R_z\left(\frac{\alpha_{l,j}}{2}, \frac{\varepsilon}{4}\right)$, then replace T and H by T^\dagger and H^\dagger , and similar for y-rotation. $R_x(\pi)$ takes $O(1)$ gate count, and $\|\mathbf{R}_{l,j} - \mathbf{R}_{l,j}(\varepsilon)\| \leq \varepsilon$. The reason of using this decomposition is that together with the controlled rotation introduced below, qubits in $\mathcal{D}_{l,j}$ can be fully uncomputed after implementing $\overline{\mathbf{C}}\mathbf{R}_{l,j}$. To be specific, $\overline{\mathbf{C}}\mathbf{R}_{l,j}$ is approximated by

$$\overline{\mathbf{C}}\mathbf{R}_{l,j}(\varepsilon) =$$


$$=$$



In our Clifford+ T circuit implementation, we just perform the following replacement in the fanin phase

$$\mathbf{R}_{l,j} \rightarrow \mathbf{R}_{l,j}(\epsilon_l), \quad \overline{\mathbf{C}\mathbf{R}}_{l,j} \rightarrow \overline{\mathbf{C}\mathbf{R}}_{l,j}(\epsilon_l). \quad (\text{S-70})$$

To analyse the decomposition accuracy, we define

$$U_l = \begin{cases} r_{0,0} \otimes \mathbb{I}_{n-1}, & l = 0 \\ \sum_{j=0}^{2^l-1} |j\rangle\langle j| \otimes r_{l,j} \otimes \mathbb{I}_{n-l-1} & 1 \leq l \leq n-1 \end{cases} \quad (\text{S-71})$$

and

$$U_l(\epsilon_l) = \begin{cases} r_{0,0}(\epsilon_0) \otimes \mathbb{I}_{n-1}, & l = 0 \\ \sum_{j=0}^{2^l-1} |j\rangle\langle j| \otimes r_{l,j}(\epsilon_l) \otimes \mathbb{I}_{n-l-1} & 1 \leq l \leq n-1 \end{cases} \quad (\text{S-72})$$

where \mathbb{I}_m is the m -qubit identity matrix. It can be verified that for ideal and Clifford+ T implementations, the final state of the output register is equivalent to

$$|\psi\rangle = U_{n-1} \cdots U_1 U_0 |0\rangle^{\otimes n} \quad (\text{S-73a})$$

$$|\psi^{(\text{CT})}\rangle = U_{n-1}(\epsilon_{n-1}) \cdots U_1(\epsilon_1) U_0(\epsilon_0) |0\rangle^{\otimes n} \quad (\text{S-73b})$$

respectively, while the QRAM has been uncomputed for both cases. We note that Eq. (S-73) is only an expression of the final state, and does not represent the actual implementation process. Because $\|U_l - U_l(\epsilon_l)\| \leq \epsilon_l$, according to the triangular inequality, we have

$$\left\| |\psi\rangle - |\psi^{(\text{CT})}\rangle \right\| \leq \sum_{l=0}^{n-1} \|U_l - U_l(\epsilon_l)\| \leq \sum_{l=0}^{n-1} \epsilon_l. \quad (\text{S-74})$$

Based on Eq. (S-74), to achieve a given accuracy $\left\| |\psi\rangle - |\psi^{(\text{CT})}\rangle \right\| \leq \epsilon$, it suffices to set

$$\epsilon_l = \epsilon / 2^{n-l}. \quad (\text{S-75})$$

2. Circuit complexity

Below, we analysis the Clifford+ T circuit complexity based on the decomposition protocol above.

Clifford+ T gate count. Each rotation $\mathbf{R}_{l,j}(\epsilon_l)$ or controlled-rotation $\mathbf{C}\mathbf{R}_{l,j}(\epsilon_l)$ accounts for $O(\log 1/\epsilon_l) = O(\log(2^{n-l}/\epsilon))$ gate count. So $\mathbf{P}\mathbf{R}$ and $\overline{\mathbf{P}\mathbf{C}\mathbf{R}}$ accounts for totally $\sum_{l=1}^n 2^l \times O(\log(2^{n-l}/\epsilon)) = O(N \log(1/\epsilon))$ gate count. Other operations during the implementation can be realized without decomposition error, and accounts for $O(N)$ gate count. Therefore, the total Clifford+ T gate count is $O(N \log(1/\epsilon))$.

Clifford+ T depth. The decomposed parallel rotation and parallel controlled-rotation accounts for $\max_l O(\log(2^{n-l}/\epsilon)) = O(\log(2^n/\epsilon)) = O(n + \log(1/\epsilon))$ circuit depth. Other operations during the implementation accounts for totally $O(n)$ depth. So the total Clifford+ T depth is $O(n + \log(1/\epsilon))$.

Clifford+ T space-time allocation. We first consider the total STA of the l th spatial layer. Each qubit is activated for time $O(n-l) + O(\log(2^{n-l}/\epsilon)) = O(n-l + \log(1/\epsilon))$. There are $O(n)$ qubits at the l th spatial layer, so the total STA is $A_l = O(2^l(n-l + \log(1/\epsilon)))$. Moreover, the STA of output register is $A_{\text{out}} = O(n) \times O(n) = O(n^2)$. Therefore, the total STA

of the algorithm is

$$\begin{aligned}
 A &= A_{\text{out}} + \sum_{l=1}^n A_l \\
 &= O(n^2) + \sum_{l=0}^n O(2^l(n-l + \log(1/\varepsilon))) \\
 &= O(n^2) + O(N) + O(N \log(1/\varepsilon)) \\
 &= O(N \log(1/\varepsilon)).
 \end{aligned} \tag{S-76}$$

The circuit complexity is summarized in Table. I of the main text.